Temporal Bone Imaging

2

Karen Nicolas and Ahmed Elsotouhy

Abbreviations

CBCT	Cone-beam CT
CPA	Cerebellopontine angle
CSF	Cerebrospinal fluid
CSOM	Chronic suppurative otits media
CT	Computed Tomography
EAC	External auditory canal
IAC	Inner auditory canal
IAC	Internal auditory canal
LSCC	Lateral semicircular canal
LVA	Large vestibular aqueduct
MDCT	Multidetector-CT
ME	Middle Ear
MRI	Magnetic Resonance Imaging
OW	Oval window
PSCC	Posterior semicircular canal
RW	Round window
SSCC	Superior semicircular canal
TB	Temporal Bone
TM	Tympanic membrane

Key Points
- The main CT Imaging modalities as MDCT and CBCT are described with advantages and inconvenients. MRI is described with its general imaging characteristics, main sequences for temporal bone imaging, and dedicated sequences for special pathologies. MRI-Contraindications are briefly reviewed.
- CT-Anatomy and MRI-Anatomy are demonstrated on several slices through the main anatomic regions of the temporal bone by both techniques.
- A systematic reading structure is proposed, that approaches the temporal bone from outside to inside, and determines for each anatomic site the essential structures to evaluate. Key images, the most adapted reconstruction plane, and pathologic manifestations at each anatomic site are described and illustrated.
- The temporal bone surfaces and surroundings are often involved by spread of temporal bone pathologies: especially infectious pathologies, as necrotizing otitis externa and chronic suppurative otitis media (CSOM) with or without cholesteatoma tend to extend beyond. Also the tegmen is a predestinated site of weakness in patients with

K. Nicolas (✉)
MEIH Hospital Mount Lebanon and Lebanese University, Beirut, Lebanon

A. Elsotouhy
Neuroradiology Department, Hamad Medical Corporation, Doha, Qatar

poor mastoid development or lysis and pathologic communications through the tegmen are described. Further entities are tumors involving the IAC or glomus tumors that have been illustrated.

- Postoperative imaging findings are briefly illustrated for ossicular reconstructions and stapes prosthesis. The important role of MRI diffusion-weighted imaging for residual/recurrent cholesteatoma is pointed out, also for associated complications to be aware of, during surgical revision. Follow-up after intervention for vestibular schwannoma is a long-term survey that needs reproducible exact measurements of slow growing residues.

2.1 Introduction

Imaging technology has greatly improved over the last two decades; high-resolution CT has been overcome by multidetector CT techniques and more recently complemented by Cone-beam CT (CBCT) with its lesser radiation and higher resolution for some middle ear structures.

MR imaging has been developed to thinner slices and 3D imaging, with specific sequences for otologic and neurotologic pathologies.

Thus, imaging nowadays is one of the basic diagnostic mainstays of temporal bone pathology to orient surgical indications and elucidate possible anatomical abnormalities. In consequence, the preoperative and postoperative counseling of the patients is rendered more informative and enlightened.

Principal imaging methods, basic anatomy, and essential imaging keys are presented.

It remains that adequate communication between the clinician and the radiologist is a prerequisite to select the best imaging protocol. Finally, the postoperative feedback from the clinician to the radiologist constitutes the main source of improvement of diagnostic expertise.

2.2 Temporal Bone Imaging Techniques

2.2.1 MDCT (Multidetector-CT)

2.2.1.1 CT Acquisition and Processing

Acquisition of a data volume of the temporal bone is actually done by slice thicknesses of 0.5–0.6 mm or less, that permit standard reformation of thin slices on each ear alone in the axial (Fig. 2.1) and coronal plane (Fig. 2.2). The standard axial plane is reached when the whole LSCC is visible on one slice (Fig. 2.1d).

Most common supplementary reformations are

- *"Axial stapes" plane*: to evaluate the whole stapes and footplate on one image (Fig. 2.3) [1].
- *Poeschl plane*: to evaluate the bony coverage of the SSCC (Fig. 2.4), if doubtful on the coronal plan.
- *Sagittal plane*: to assess relation from malleus head and anterosuperior wall of the tympanic cavity.

  Injection of iodine contrast is almost never required, except for suspected vascular lesions.
- Advantages of MDCT: short examination time, modality almost everywhere available, providing an overall view on the two temporal bones, the nasopharynx, most parts of the sinuses, and the base of skull.
- Inconvenients of MDCT: Considerable radiation exposure, especially in children, and important metallic artifacts from several prosthesis or cochlear implants.

2.2.2 CBCT (Cone-Beam CT)

It is a recent imaging method based on a cone of radiation turning around the patient (instead of the X-ray fan beam rotating spirally around the patient). Preliminary results of institutions that use already CBCT in their daily practice confirm its utility [2] and further implementation as a second and complementary imaging method is predictable.

2.2.2.1 Advantages

- Radiation is less (several former studies estimated the difference at least 3–10 times less
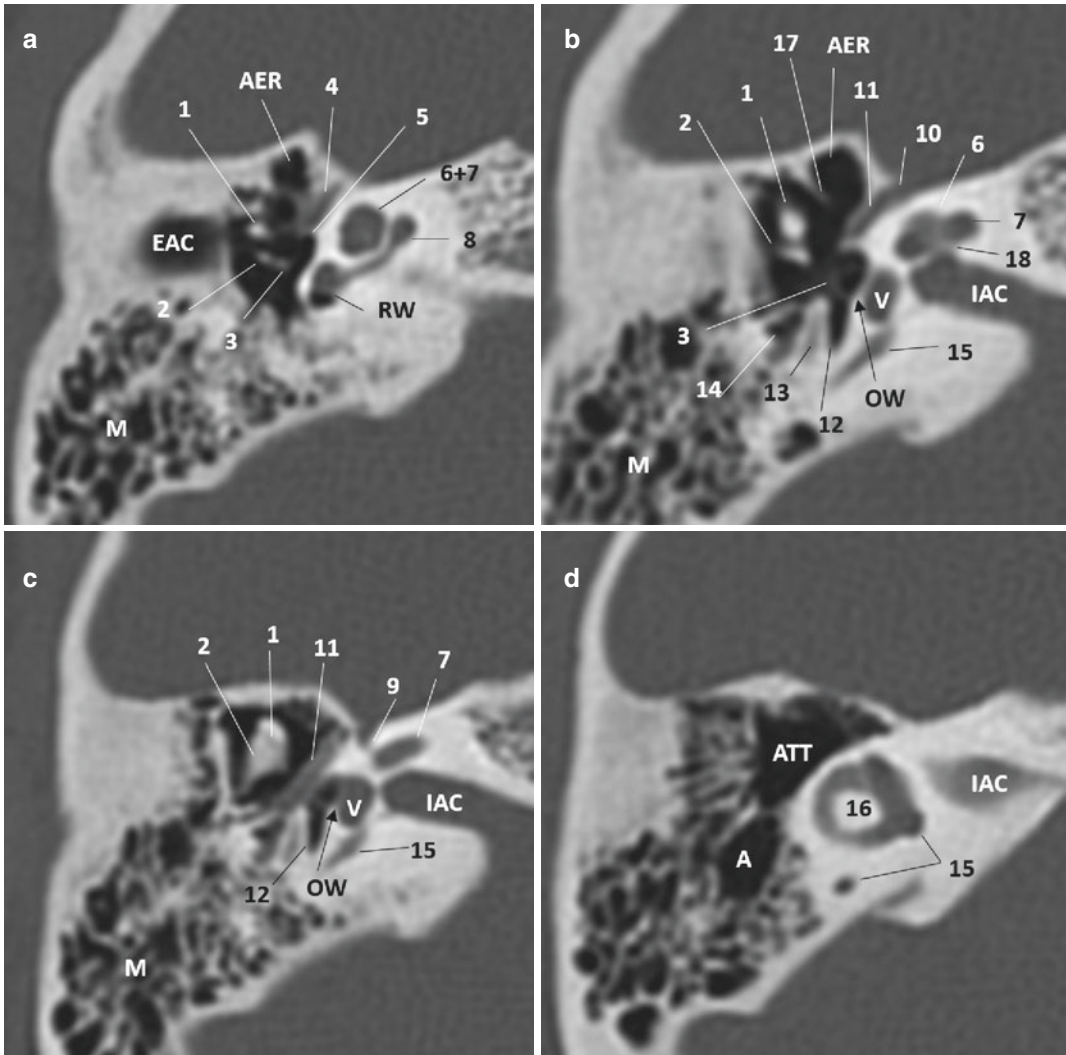
Fig. 2.1 Main anatomic structures on consecutive axial CT cuts from **a** to **d** of the middle ear from caudal to cranial. (1) Malleus, (2) Incus, (3) Stapes, (4) Tensor tympani muscle, (5) Cochleariform process, (6) Last turn cochlea, (7) Mid turn cochlea, (8) Basal turn cochlea, (9) Labyrinthine portion N VII, (10) Geniculate ganglion, (11) Tympanic portion of N VII, (12) Sinus tympani, (13) Stapedial muscle, (14) Facial recess, (15) PSCC, (16) LSCC (standard plan), (17) Cog, (18) Modiolus. *AER* anterior epitympanic recess, *EAC* external auditory canal, *M* mastoid, *RW* round window, *IAC* internal auditory canal, *V* Vestibule, *OW* oval window, *A* antrum, *ATT* attic

for CBCT versus MDCT [3, 4]), but exact evaluation of radiation dose is much difficult, probably underestimation of the CBCT dose because of its beam geometry that cannot be fully evaluated by the standard dose evaluation of MSCT [5–7].

• Strikingly higher spatial resolution for interfaces with high difference of density (air-bone or air-tissue-contrast) has been shown, especially in cadaveric specimen [8, 9] with excellent visibility of ossicular chain and articulations [10], also cochlear anatomy and the facial nerve.

• Much less metallic artifacts than MDCT [8, 11] predestinating CBCT for prosthesis and cochlear implant controls [12].
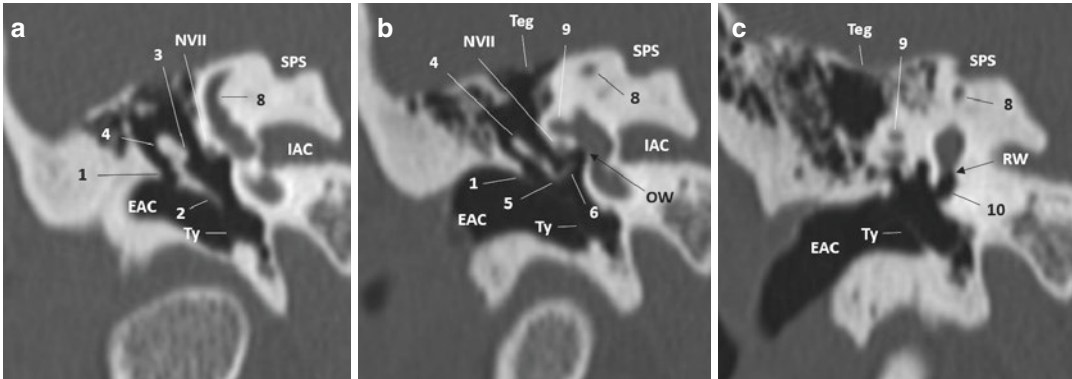
Fig. 2.2 Anatomy on coronal CT slices from **a** to **c** from anterior to posterior: (1) Scutum, (2) Malleus handle, (3) Malleus neck, (4) Incus body, (5) Incudo-stapedial joint, (6) Stapes, N VII facial nerve, (8) SSCC, (9) LSCC, (10) Recess towards the round window. *EAC* external auditory canal, *Ty* tympanic membrane, *IAC* internal auditory canal, *SPS* superior petrosal sinus, *OW* oval window, *RW* round window, *Teg* tegmen
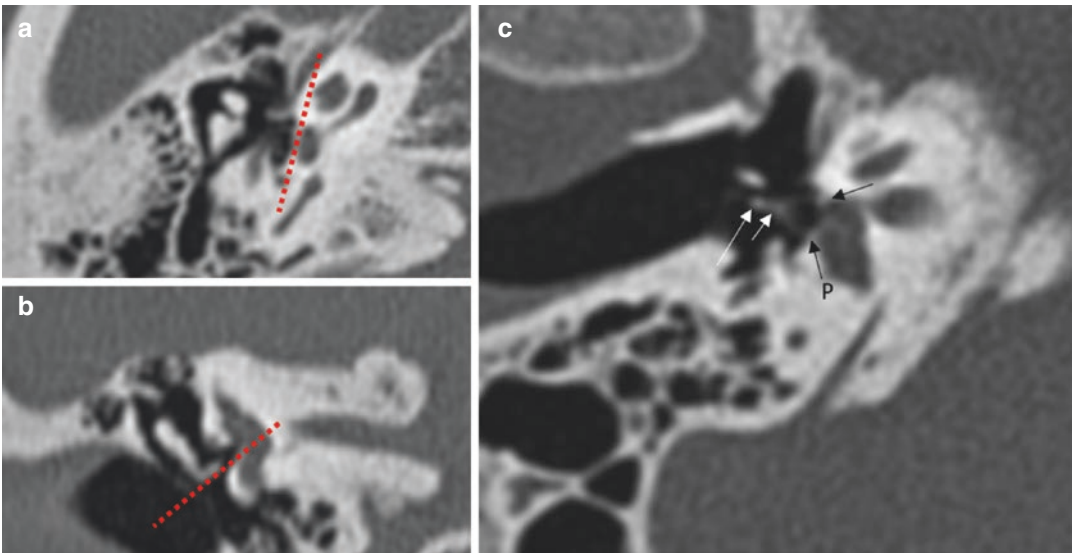

Fig. 2.3 Axial stapes plan: (**a**) on axial CT, the red reference parallel to the footplate for reconstruction → obtain (**b**): Second red reference line along the stapes axis (red dotted line) → obtain (**c**): axial stapes plan with the whole stapes on one slice. Thin footplate (P) between the two black arrows

2.2.2.2 Inconvenients

- Although CBCT has high specificity for otosclerosis, its sensitivity for inactive, sclerotic foci was found to be very low [13]. Others stated that more fenestral lesions were found by MSCT than by CBCT, whereas retrofenestral lesions were equally diagnosed by both techniques [14].
- Lack of soft-tissue contrast resolution limits the use of CBCT in general diagnostic imaging of the temporal bone [10].

- Small field of view enables only one side examination per acquisition.

2.2.3 MR Imaging

2.2.3.1 General MR Imaging Characteristics

- 1.5 Tesla MRI, most available and providing a good standard image quality and evaluation of any anatomic region of head and neck.
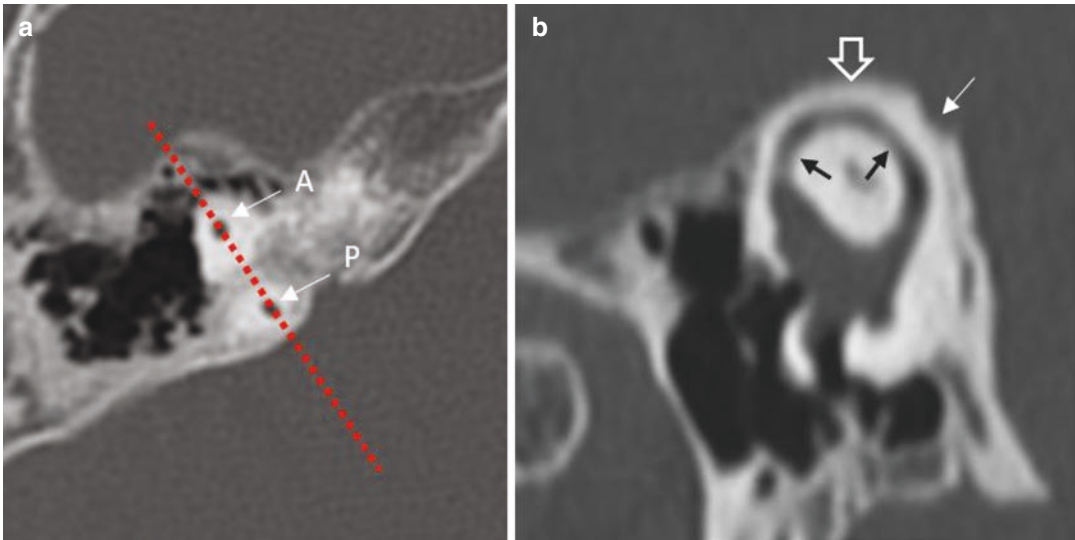
Fig. 2.4 (**a**) Poeschl Plan: axial CT through the upper TB, above the level of axial CT slices of Fig. 2.1d. Red reference line through the anterior (A) and posterior (P) limb of the

SSCC for reconstruction → obtain (**b**) the whole SSCC on one slice (small black arrows), the bony coverage (empty arrow) can be assessed. Superior petrosal sinus (white arrow)

- 3.0 Tesla MR using a higher magnetic field strength and providing overall higher imaging quality and newer sequences (see Sect. 2.2.3.2).
- MR is a nonirradiating imaging method using radiofrequency pulses and gradients [15] providing a highly superior soft-tissue characterization in comparison to CT.
- Terminology: different shades of gray on the image are described as follows:
  - white as *high signal intensity*.
  - gray as *intermediate signal intensity*.
  - black as *low signal intensity*.
- Standard sequences are T1-, T2-weighted, or Flair (fluid attenuated) sequences.
  - *T1w*: liquid (as CSF) is hypointense, fat is hyperintense.
  - *T2w*: liquid (as CSF) is hyperintense, fat is also hyperintense.
  - *Flair*: CSF is hypointense, inflammatory or proliferative tissues are hyperintense.
- Gadolinium contrast administration (intravenous) is used to search for pathologic hyperintense contrast uptake on *T1w sequences with fat suppression* (the normally hyperintense fat signal becomes hypointense and permits better discrimination of the contrast uptake) in case of

  - Suspected vascular tumors in the middle ear cavity or around the jugular foramen,
  - Labyrinthitis, acute mastoiditis, lesions in the internal auditory canal (IAC)/cerebellopontine angle (CPA)

2.2.3.2 Dedicated Sequences for Temporal Bone Imaging

High-Resolution 3D T2-Weighted Sequence (3D Drive/CISS/FIESTA/etc.)

This is the essential sequence for middle and inner ear imaging because of high spatial resolution due to inframillimetric slice thickness. It shows

- High contrast between the hypointense vestibulocochlear and facial nerve bundles along their trajectory through the IAC and the hyperintense CSF in the IAC
- The normally hyperintense fluid signal of the membranous labyrinth or pathologic loss of signal
- Different signal intensities for different fluid or solid middle ear pathologies.

Diffusion-Weighted Imaging (DWI)

Diffusion imaging is based on the random Brownian motion of water molecules in a voxel

of tissue. If their free motion becomes reduced, a restricted diffusion appears. The *B* value indicates the degree of diffusion weighting applied, starting by B0 and raising up to mostly B1000 s/mm^2. The ADC value (apparent diffusion coefficient) is calculated as B0–B1000, appearing black in case of a positive restriction, white in absence of restriction.

In the middle ear cleft, cholesteatoma was found to be the almost unique pathologic condition that exhibits diffusion restriction. DWI technics are continuously improving. Numerous studies [16, 17] confirmed the advantages of non-echoplanar DWI techniques over previous echoplanar techniques for the detection of cholesteatoma (minimal detection size actually of 2 mm).

3D Flair Imaging 4 h Delayed After Gadolinium Injection for 3 T MRI

This imaging technique has been proposed already since 2009 [18] and continuously improved [19] and implicated in daily imaging routines with 3 T MRT. Recently [20], the combined analysis of vestibular endolymphatic hydrops and perilymphatic enhancement of the cochlea gave combined sensitivity of 79.5% and specificity of 93.6% for Menière's disease.

2.2.3.3   Contraindications

- Foreign metallic bodies in the eye represent an absolute contraindication.
- Cochlear implants represented for longtime an absolute contraindication for MRI, but implants with easier access to MRI have been very recently FDA approved and will be subject of further innovations.
- Prosthesis made of nonmagnetic metals and alloys, including titanium, platinum, and tantalum, showed no potential for movement and were safe by 1.5 Tesla MRI and all above [21].
  Exception: Stainless steel prostheses (mainly used in the years 1960s and 1970s) have been shown to move in several experiments, and their MRI safety may be compromised [22].

2.3   Cross-Sectional Anatomy of the Temporal Bone

2.3.1   Cross-Sectional CT-Anatomy

The temporal bone (TB) is embryologically composed by the fusion of four different bones that are the petrous bone, squamous bone, tympanal bone and styloid bone. The fusion lines of these different parts persist in form of visible sutures on rather all CT-Scans, not to be confused with fracture lines!

Basic sectional views on the most important anatomical structures on the axial, coronal view, the axial stapes plan [1] and the Poeschl plan are shown in the following figures (Figs. 2.1, 2.2, 2.3, and 2.4) [23].

2.3.2   Cross-Sectional MR-Anatomy

Only 3D high-resolution T2-weighted images (Drive, CISS, FIESTA, etc.) with inframillimetric slice thickness show the trajectory of the seventh and eighth cranial nerves inside the IAC in detail (Fig. 2.5). At the "Bill's bar" at the fundus of the IAC, the facial nerve runs in the anterosuperior segment, the cochlear nerve in the anteroinferior segment, and the superior and inferior vestibular nerves in the posterior segments (mnemonic: 7up & Coke Down) (Fig. 2.5c). The different turns of the cochlear and the semicircular canals are well individualized on T2w images due to their liquid components (Fig. 2.6).

2.4   Systematic Reading of Temporal Bone Structures Imaging and Most Frequent Pathologies

In general, CT is the first imaging method of investigation of the outer ear and the middle ear structures. The osseous labyrinth is well seen by CT as by MRI, whereas MRI is the leading imaging method for the content of the membranous labyrinth, the IAC, and all condensation images of the mastoid and tympanic cavity, that are clinically doubtful for complicated infectious disease or cholesteatoma.

A systematic evaluation of the temporal bone can be done along the following steps
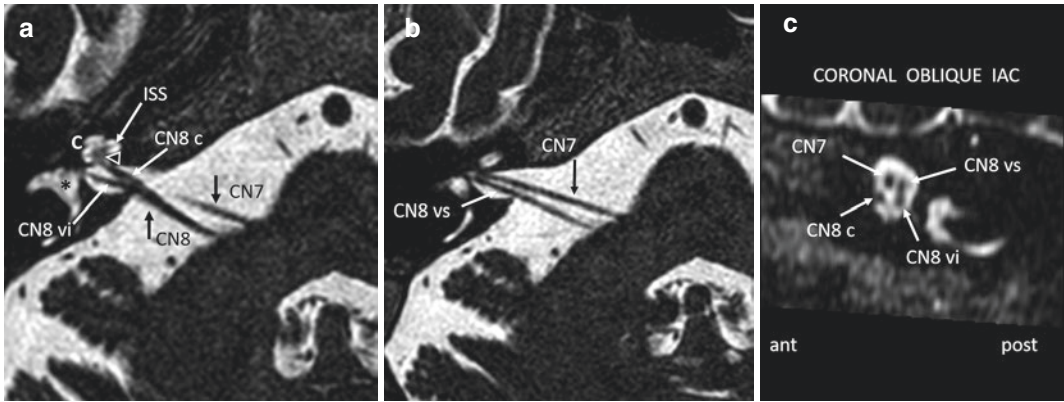
Fig. 2.5 (**a**) Transversal 3D HR T2w Drive image at inferior part of the IAC, (**b**) at upper part of the IAC, (**c**) coronal oblique reformation perpendicular to the lateral end of IAC. Different nerves: CN7 facial, CN8 vestibulocochlear bundle, CN8vi vestibularis inferior, CN8vs vestibularis superior, CN8c cochlear. Interscalar septum (ISS), vestibule (asterisk), cochlea (C), modiolus (empty triangle)
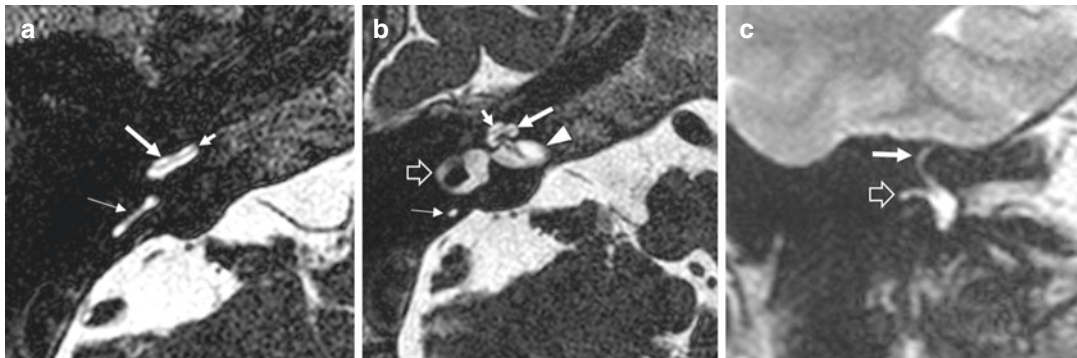

Fig. 2.6 (**a**) Transversal MRI 3D HR T2w Drive image inferior to the IAC: basal cochlear turn (thick long arrow), ISS interscalar septum (short arrow), inferior limb of the PSCC (thin arrow). (**b**) Slightly cranial to (**a**) at level of IAC: mid cochlear turn (thick long arrow), last cochlear turn (small arrow), LSCC (empty arrow), PSCC (thin arrow), IAC (arrowhead). (**c**) Coronal MRI T2w: lateral limb of SSCC (white arrow) and LSCC (empty arrow)

progressing from the outer to the inner ear structures, mentioning for each structure main pathologies and their aspects.

2.4.1 External Auditory Canal (EAC)

- Osseous borders: discontinuity by *persistent foramen of Huschke*, traumatic, or erosive (*infectious or tumoral* origin)
- Scutum (to analyze in the coronal plan!): It is the upper medial bony limit of the tympanic bone, on which the pars flaccida of the ear drum inserts: intact (Fig. 2.2) or amputated (Fig. 2.9a), amputation may indicate an *acquired cholesteatoma*.

- Skin: focally or generally thickened, to refer to the clinical context and inspection as in *external necrotizing otitis* (Sect. 2.5.1.2).

2.4.1.1 *EAC Stenosis or Atresia*
EAC atresia can be completely or incompletely atretic. A number of key points should be looked for [24]:

- Width of the middle ear cavity (should be >3 mm to be suitable for surgical indication [25])
- Stapes malformations: present or not; often associated with a lack of oval window formation.
- VII course identification (Fig. 2.7).
- Look for congenital cholesteatoma behind the atresia plate.

2.4.2 Tympanic Membrane (TM)

Exclusive role of CT
- Tympanic membrane retraction towards the cavity [26]:
  - If close contact to the incudostapedial chain, focal lysis of the joint can be observed (Fig. 2.8a).
  - If retracted on the middle attic wall, it can be very close to the tympanic facial nerve canal (Fig. 2.16a).

- *Perforation:* size and site, central or marginal (Fig. 2.8b).
- Thickening or *myringosclerosis* (Fig. 2.8c).

2.4.3 Tympanic Cavity

The tympanic cavity has a complex anatomy, with numerous osseous limits to analyze and ways of communication with the nasopharynx by the Eustachian tube, with the mastoid by the
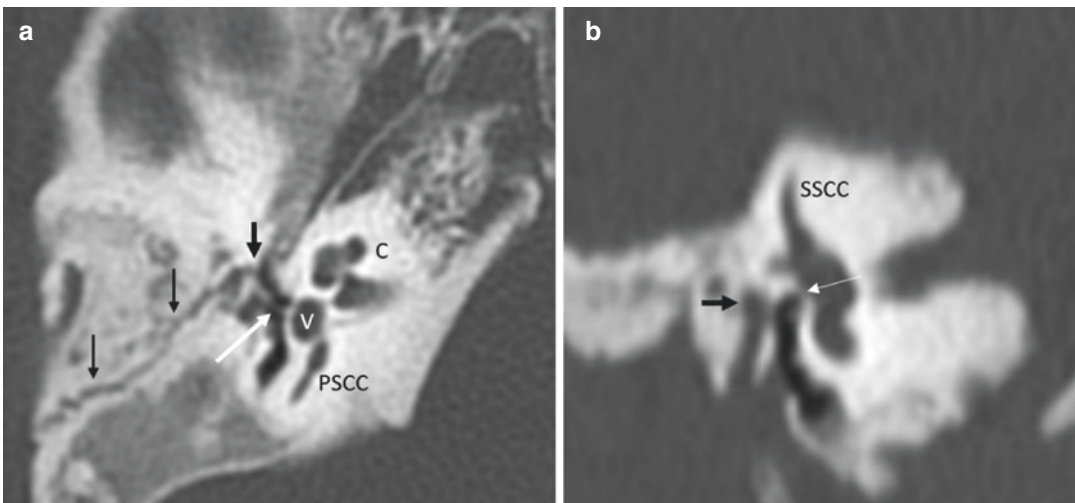

Fig. 2.7 (**a**) Axial CT: Complete atresia of EAC, tympanic bone absent, petrosquamous suture (black arrows). Small cavity (short black arrow) with rudimentary ossicular chain, stapes present (white arrow). Normal inner ear structures (C cochlea, V vestibule, PSCC). (**b**) Coronal CT: horizontal portion of VII (black arrow) advanced at level of the oval window (white arrow)
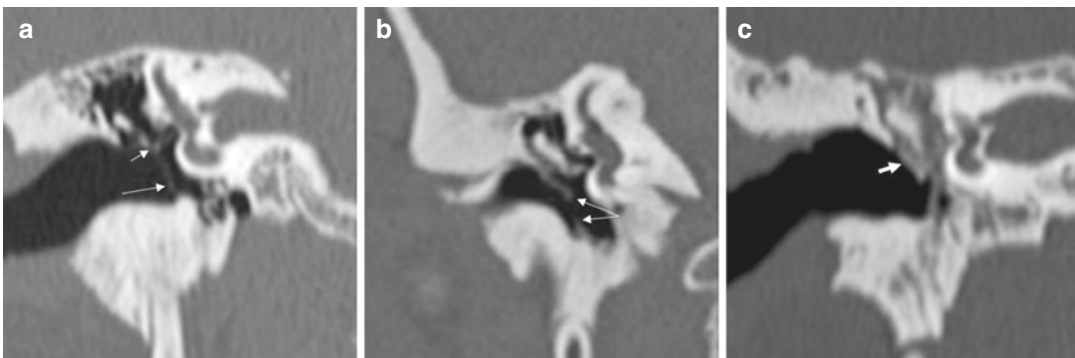

Fig. 2.8 Coronal CT: (**a**) thin TM (arrows) retracted on incudostapedial joint with focal lysis (small arrow). (**b**) Perforation (between arrows) of the thickened TM. (**c**) Myringosclerosis (arrow)

aditus ad antrum, and with the otic capsule via the oval and round windows (Figs. 2.1 and 2.2).

The most frequent pathologies are infectious or inflammatory diseases that concern the tympanic cavity and contents and may extend to all adjacent structures.

Major role of CT
- Aeration/condensations (special look for the different recesses as AER, sinus tympani).
- Bony walls (intact/dehiscent/lytic) especially the tegmen (coronal plan, Fig. 2.2b).
- Tegmen slope (sagittal plan [27]).

2.4.3.1 *Cholesteatoma*
Most often, cholesteatoma is a clinically established diagnosis.

Role of CT: Typical bony erosions are best demonstrated by CT (amputation of the scutum, or the cog), and/or typical rounded or irregular lobulated condensation images in the tympanic cavity (Fig. 2.9a) with adjacent ossicular chain lysis (Fig. 2.9a,b). Bony walls look smoothened in contact with a complete condensation of the lumen of antrum and/or tympanic cavity and disappearance of visible trabeculations (Fig. 2.9c). Erosion of the bony limit of the LSCC is another sign of bony lysis, important to be known before surgery.

Role of MR: Diffusion images have shown sensitivities from 0.86 to 0.93 and specificities

from 0.88 to 0.97 for detection of cholesteatoma in large meta-analysis in 2013 and 2017 [28, 29]. Sensitivities range around 90–100% to detect cholesteatoma as small as 2 mm [30].

Especially if the condensations concern the AER, a hidden space for otoscopic evaluation, CT may show condensations and the disappearance of the cog (Fig. 2.10a).

MR permits to confirm the small cholesteatomatous process in the AER (Fig. 2.10b–d).

2.4.4 Ossicular Chain

Exclusive role of CT
- Topography of the ossicles.
- *Post-traumatic discontinuity*, most often incudostapedial (Fig. 2.11a), less frequently incudomallear (Fig. 2.11b), rarely stapedial fractures (axial stapedial plan! (Fig. 2.11c)).
- *Fixity of the ossicular chain* can be congenital, as the malleus bar, that is fixing the malleus to the anterior attic wall (Fig. 2.12a), or due to a malformative attachment of the ossicular chain, as a hypoplastic incus that is retracted to the Fallopian canal (Fig. 2.12b), or a malformed hypoplastic stapes inserting on a very dense footplate (Fig. 2.12c).
- Fixity can also be acquired, as a result of postinflammatory reaction inside the tympanic cavity, as by tympanosclerosis that can involve
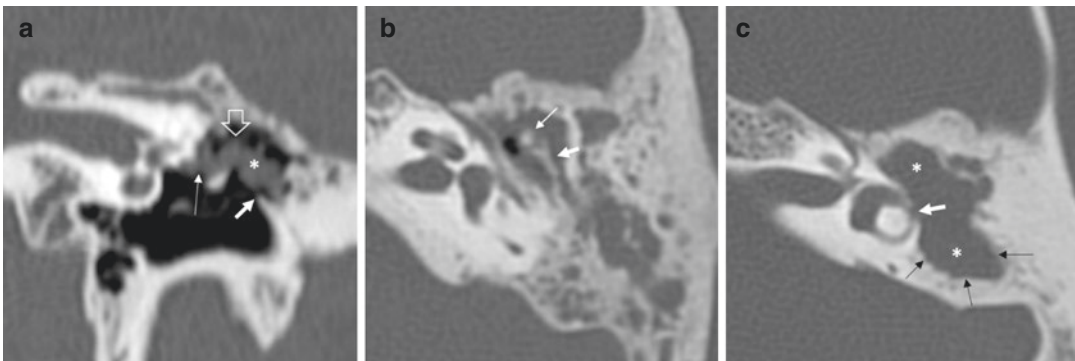

Fig. 2.9 (**a**) Coronal CT: amputation of scutum (short white arrow), irregular attical lobulated soft-tissue mass (asterisk) in contact with the VII (long arrow), advanced lysis of ossicles (empty arrow). (**b**) Axial CT: partial lysis of malleus head (thin arrow) and advanced lyses of incus (thick arrow). (**c**) Complete condensation of the atticoantral spaces (double asterisks) with smoothening of the borders (black arrows), erosion of LSCC (white arrow)
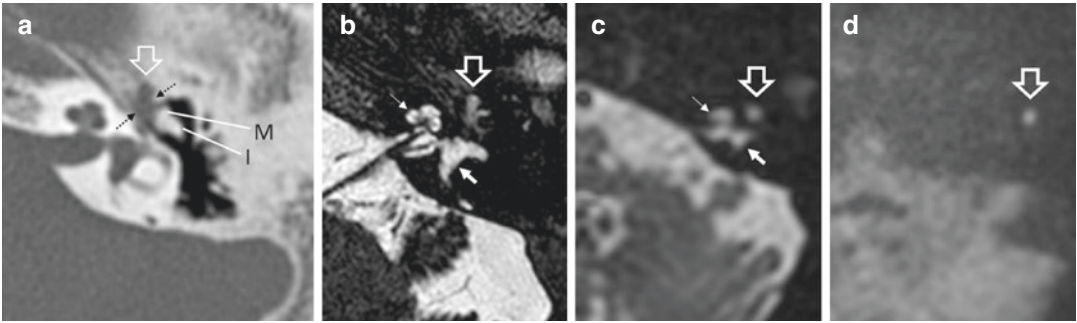
Fig. 2.10 Small cholesteatoma invading the AER. (**a**) Axial CT: soft-tissue mass in the AER (empty arrow), associated to probable lyses of the cog (should be an osseous ridge between dotted arrows). *M* malleus head, *I* incus. (**b**) Axial MRI HR T2 Drive, (**c**) Diff w B0 image: (**d**) Diff w B1000 image: AER (empty arrow) cochlea (slim arrow), vestibule (thick arrow), positive restriction only in the AER in (**d**), very specific for cholesteatoma

Fig. 2.11 (**a**) Coronal CT: discontinuity of incudostapedial joint (empty arrow), (**b**) axial CT: discontinuity of incudomalleal joint (empty arrow). (**c**) Axial CT reconstruction in stapes plan: discontinuity between distal crura of the stapes (white arrows) and footplate (between black arrows)
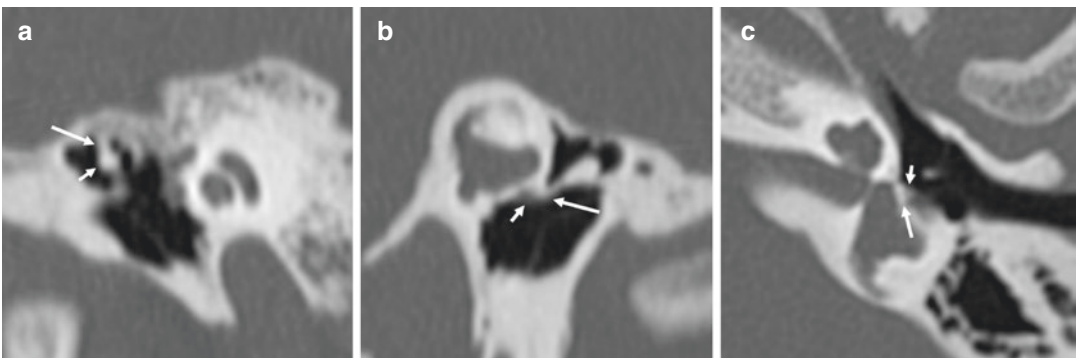

Fig. 2.12 Ossicular chain fixities: (**a**) coronal CT: large bony attachment (long arrow) of malleus head (short arrow) to the tegmen. (**b**) Coronal CT: hypoplastic long process of the incus (long arrow) attached on the Fallopian canal (short arrow). (**c**) Axial CT: hypoplastic stapes with very short crura (short arrow) inserting on a thick and very dense footplate (long arrow)
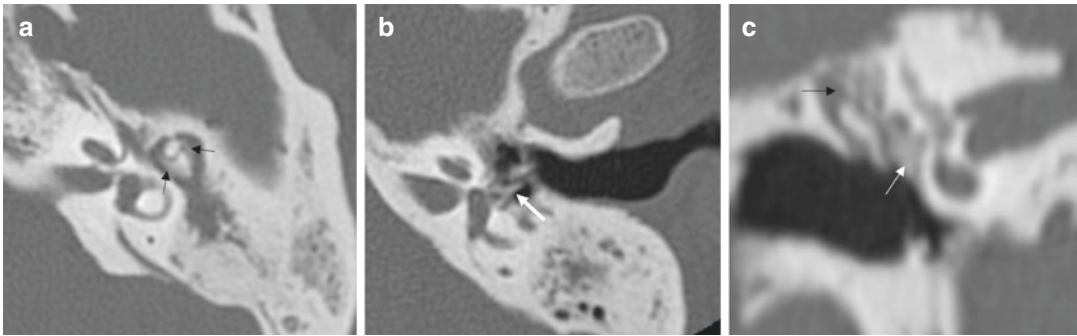
Fig. 2.13 Tympanosclerosis: axial CTs: (**a**) typical periarticular calcifications (arrows) of incudomallear joint, (**b**) important thickening and hyperdensity of stapes superstructure (arrow). (**c**) Coronal CT with diffuse calcified condensations of oval window niche (white arrow) and inner attic (black arrow)

the malleolar complex alone, the stapedial complex alone, or the whole cavity with malleus and stapedial fixity [31] (Fig. 2.13).

2.4.5   Oval Window

- Oval window niche (normal height or reduced).
- *Hypoplasia* of the oval window.
- Footplate: normal thickness, or thickening (to evaluate on axial stapes plan! (Fig. 2.3), especially in pathologies like *otosclerosis, stapedial ankyloses, or tympanosclerosis* [31].
- Fissula antefenestram situated immediately anteriorly to the anterior wall of the oval window is the most common site for *otosclerosis* (Fig. 2.14a).

Major role of CT: high specificity and sensitivity (over 90%) [32] for typical foci of otosclerosis in the fissula antefenestram, for pericochlear extension (Fig. 2.14b) with or without contact to the cochlear endosteum, calcifications of cochlear turns as sign of advanced stage. Classification systems in use according to Veillon [33], or Symons and Fannings [34] especially for more advanced stages.

2.4.6   Round Window

Major role of CT: The round window represents the contact face between the middle ear cavity and the scala tympani of the cochlea. Otosclerosis of the round window is not rare, observed in up to 13% of patients with otosclerosis. A radiologic classification of RW invasion and their audiological impacts has been established [35].

- Round window membrane partially or completely thickened (Fig. 2.14d).
- Round window recess accessible or obliterated (Fig. 2.14e).
- Round window hypoplastic (Fig. 2.14f).

2.4.7   Facial Nerve

The facial nerve has a complex trajectory from its origin at the lateral pons, its cisternal portion traversing the CPA, labyrinthine portion until the geniculate ganglion, the horizontal tympanic portion along the medial attic wall until the second genu, and the vertical mastoid portion through the mastoid until the stylomastoid foramen (Fig. 2.15). Need for axial and coronal images to assess the whole trajectory.
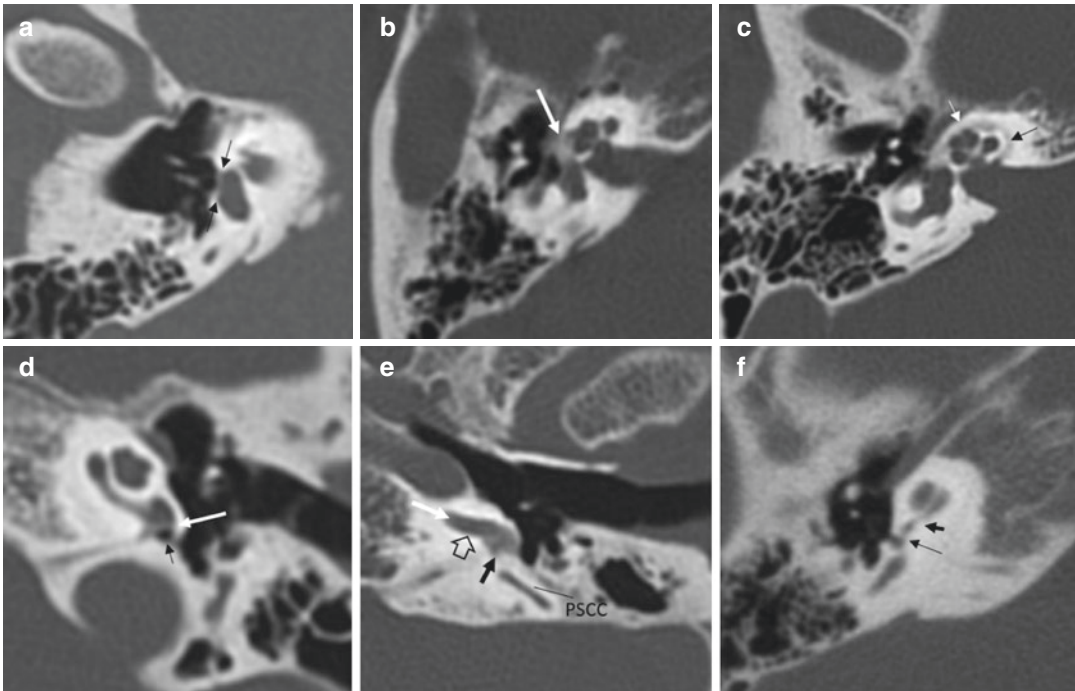
Fig. 2.14 Axial CT (**a**) axial stapes plan: global thickening of the footplate (between black arrows). (**b**) Large otosclerotic focus of the fissula antefenestram (arrow), already in close contact with the cochlear endosteum. (**c**) Extended pericochlear otosclerosis, partially in close contact with the endosteum (white arrow), some foci stay at distance of the endosteum (black arrow). (**d**, **e**) Axial CTs of round window otosclerosis, in (**d**) thickened round window membrane (white arrow), round window recess aerated (thin black arrow). (**e**) Typical otospongiotic focus obliterating the whole round window recess (black arrow): RW4. Scala tympani (empty arrow), spiral ligament (long white arrow). (**f**) Hypoplastic round window (long arrow), stenotic proximal basal turn (short arrow)

- TM can be retracted on the VII canal (Fig. 2.16a).
- Second portion with normal position in the canal, or overhang, coming in contact with the ossicular chain or not (Fig. 2.16b).
- Bony canal integrity of the second and third portions or erosion (Fig. 2.16c).
- An enlarged angle between the first and second portions is observed in cases with X linked deafness or cochlear hypoplasia type IV, strongly associated with Gusher syndrome (Fig. 2.21c) [36].

2.4.7.1 *Facial Nerve Paralysis*

Role of CT: maybe the exam of first approach, to eliminate any gross pathology along the temporal facial nerve trajectory.

MRI is the method of choice: essentially with injected T1 sequences to analyze the facial nerve trajectory from the brainstem to the fundus of the internal auditory canal and to visualize soft-tissue lesions along the lateral course of the nerve.

- A normal facial nerve faintly enhances in the geniculate ganglion, tympanic, and mastoid segments.
- In *Bell's palsy*, there is enhancement of the cisternal and labyrinthine segments, and greater degree of enhancement in, geniculate ganglion, tympanic, and mastoid segments.
- *VII schwannoma*, the most frequent tumoral pathology of this nerve, shows strong contrast enhancement.
- *Hemangiomas* of the facial nerve typically occur at the geniculate ganglion and show also avid contrast enhancement. [37].
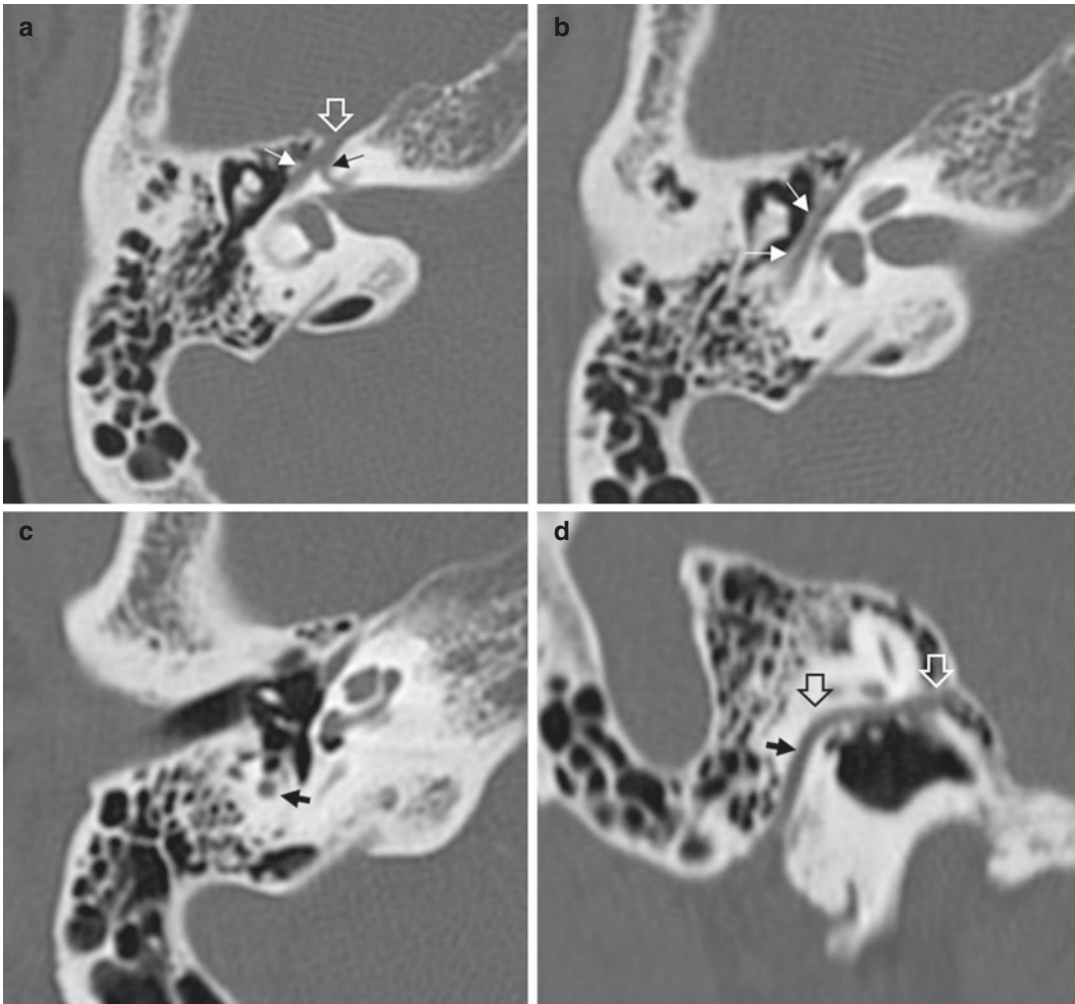
Fig. 2.15 Facial nerve trajectory on axial CT from cranial to caudal (**a–c**) and (**d**) oblique reconstruction along the tympanic and mastoid segments: (**a**) First labyrinthine segment (black arrow), geniculate ganglion (empty arrow), proximal tympanic segment (white arrow), *note here the normal small angle between the first and second portion of the facial nerve.* (**b**) Tympanic segment (arrows), (**c**) mastoid segment (arrow), (**d**) third mastoid segment (black arrow), second genu (black empty arrow), geniculate ganglion (empty white arrow)

2.4.8 Mastoid and Sigmoid Sinus

The pneumatization status of the mastoid (Fig. 2.17) as well pneumatized, diploic, or sclerotic informs about a predisposing condition for infectious and inflammatory pathologies.

The aeration status characterizes the absence or presence of condensations and their distribution in the middle ear cleft: one axial key image through the long axis of the incudomallear chain shows AER, Attic, and Antrum on the same slide (Fig. 2.17a) that are indicative of infection or inflammatory process [38].

- Trabeculations are preserved or lytic.
- Sigmoid sinus is normal or anteriorly positioned.
- Jugular bulb situation position is normal or high.
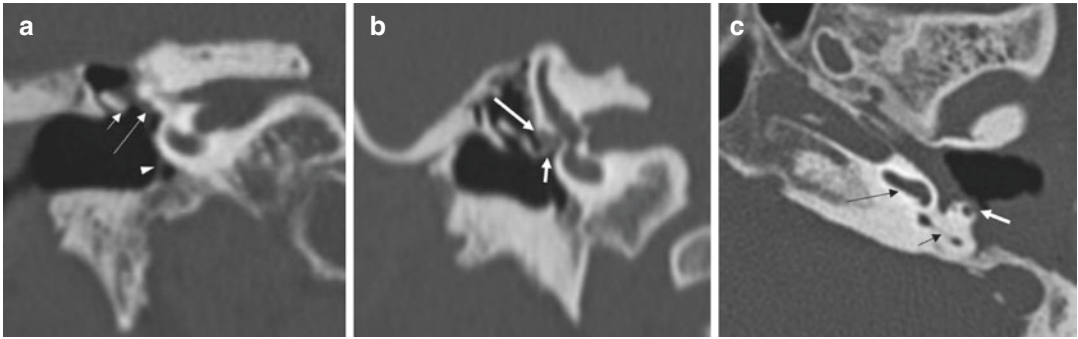- Shape of tegmen slope (on coronal and sagittal images).

Fig. 2.16 Coronal CT (**a**, **b**): (**a**) TM retraction on the incus (small arrow), and tympanic VII (long arrow), inferior retracted TM (arrowhead). (**b**) Prominent VII (long arrow), in close contact to stapes superstructure (short arrow). (**c**) Erosion of the mastoid segment of the VII (white arrow) inferior to the second genu, in contact with large condensations in mastoidectomy cavity. Basal cochlear turn (long black arrow), PSCC (short black arrow)
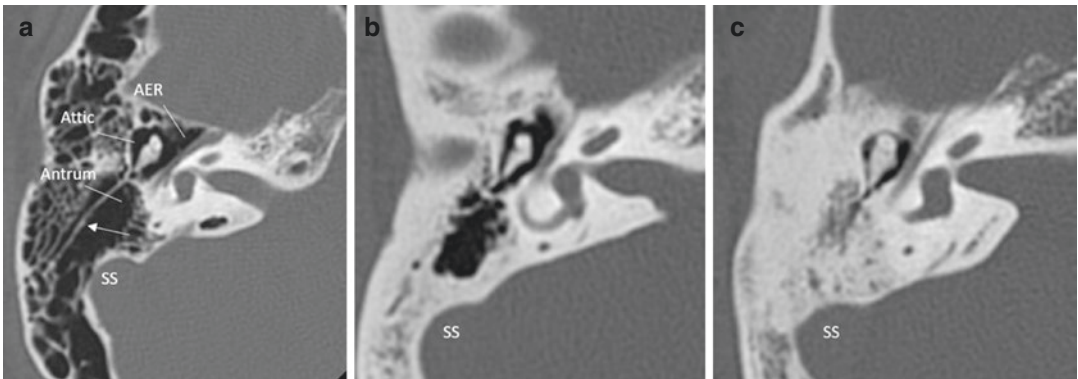

Fig. 2.17 Mastoid-pneumatization status: (**a**) well pneumatized, see the AER, Attic, and Antrum on the same slide, additional finding a Koerner septum (arrow). (**b**) Diploic, (**c**) sclerotic. *SS* sigmoid sinus

2.4.9 Petrous Apex

The internal auditory canal bisects the petrous apex into a large anterior portion that typically contains bone marrow and a smaller posterior portion that is derived from the otic capsule.

Role of CT
- Evaluation of the development of the petrous apex: Sclerotic or pneumatized or filled with condensation images.
- Expansile lesion, preserved limits, or destructive (Fig. 2.18).

Role of MRI: In case of expansile bone erosion, MR may identify the content. *Cholesterol granuloma* is the most common lesion arising in the petrous apex. Classically, it occurs in a pneumatized petrous apex and a long-standing history of ME cleft dysventilation syndrome. MRI is specific for the diagnosis with hyperintense signal on T1 and T2, no contrast enhancement. A hypointense rim on T2-weighted images may be present, which is due to hemosiderin or a preserved rim of bone [39].

In asymmetric petrous apex pneumatization with a unilaterally nonpneumatized apex, its spongiotic signal intensity similar to the clivus on different MRI sequences is also relatively high on

T2- *and* T1-weighted images and should not be mistaken for cholesterol granuloma (Fig. 2.19). The pneumatized side is most often devoid of signal due to the aeration, or shows condensation.

Other lesions are *cholesteatoma*, *cephalocele*, *petrous apicitis* (*Gradenigo syndrome*), or

Fig. 2.18 Axial CT showing an expansile soft-tissue lesion in the petrous apex (thin arrows), surrounded by a thickened cortical bone, and continuous extension (short arrow) into the tympanic cavity (asterisk). Normal left petrous apex with some aerated cells (empty arrow)

petrous carotid aneurysm. Benign and malignant tumors, other vascular lesions, fibrous dysplasia-can affect the petrous apex.

2.4.10 Cochlea

Normal development with a spiral structure of 2½ to 2¾ turns and visibility of the osseous spiral lamina separating scala tympani from scala vestibuli on CT and MRI. The modiolus should also be recognized (Fig. 2.1b).

2.4.10.1   *Cochlear Anomalies*

Jackler et al. [40] made the first classification of *inner ear malformations*. Since 2002, Sennaroglu proposed an adapted classification [41] from the complete aplasia of the membranous labyrinth (Michel deformity) and common vestibulo-cochlear cavity to different types of incomplete partition.

They are important to distinguish, because their therapeutical approach is different (Fig. 2.20) [42].

CT and MRI have similar value to detect morphologic anomalies of the osseous labyrinth.
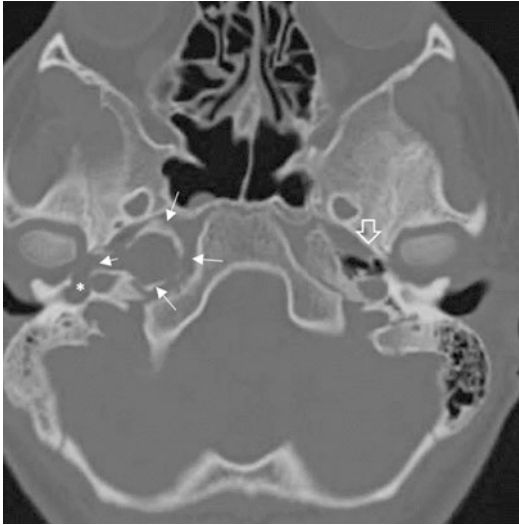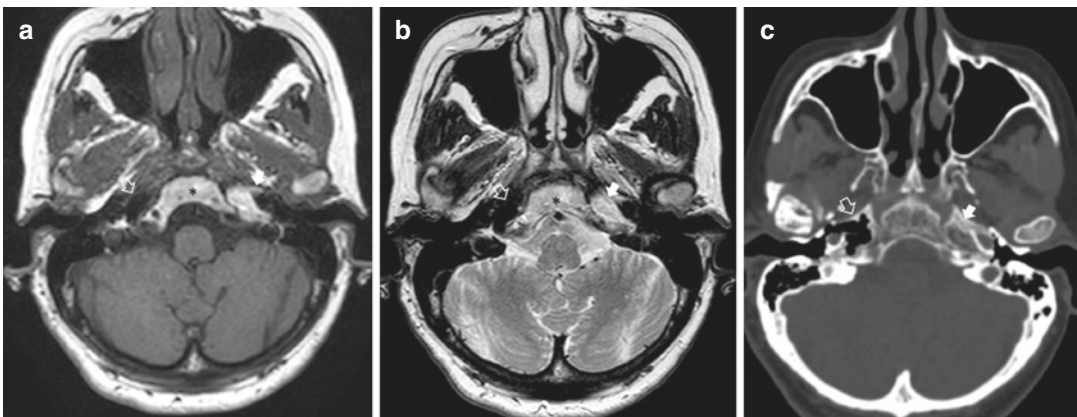
Four additional types of *cochlear hypoplasia* are

Fig. 2.19 (**a**) Axial T1w and (**b**) axial T2w MR images show high density of the left petrous apex (plain arrows), with equal density to the bone marrow of the clivus (asterisk). Well pneumatized right petrous apex devoid of signal (empty arrows). (**c**) Axial CT: well pneumatized right petrous apex (empty arrow), nonpneumatized spongiotic petrous apex on the left (plain arrow)
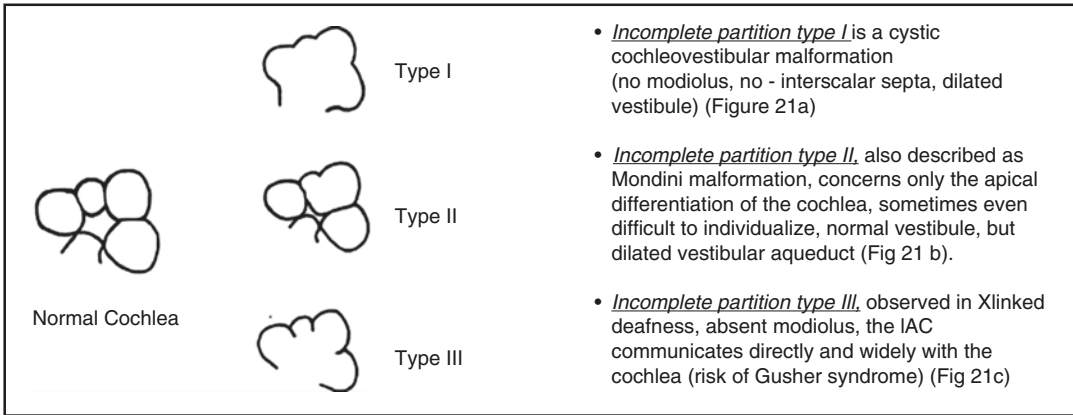
Type I

- *Incomplete partition type I* is a cystic cochleovestibular malformation (no modiolus, no - interscalar septa, dilated vestibule) (Figure 21a)

- *Incomplete partition type II,* also described as Mondini malformation, concerns only the apical differentiation of the cochlea, sometimes even difficult to individualize, normal vestibule, but dilated vestibular aqueduct (Fig 21 b).

Normal Cochlea

Type II

- *Incomplete partition type III,* observed in Xlinked deafness, absent modiolus, the IAC communicates directly and widely with the cochlea (risk of Gusher syndrome) (Fig 21c)

Type III

Fig. 2.20 Representation of different types of congenital cochlear malformations with incomplete partition according to Sennaroglu [42]
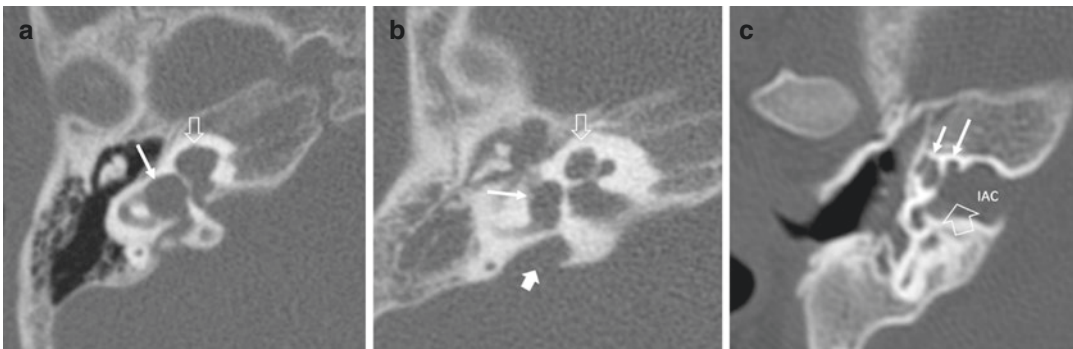

Fig. 2.21 Incomplete partition (**a**) type I: cystic cochleo-vestibular malformation, cochlea: empty arrow, vestibule: arrow, (**b**) type II (Mondini): apical incomplete partition (empty arrow), almost normal vestibule (white arrow), LVA (plain arrow). (**c**) Type III (x-linked deafness): large IAC, communicating widely (empty arrow) with the basal turn of the cochlea (long arrow), no modiolus! Mid and apical turns of cochlea (short arrow)

- *Type I* budlike, hypoplastic cochlear bud (Fig. 2.26b).
- *Type II* cystic hypoplastic cochlea without modiolus but with enlarged vestibular aqueduct.
- *Type III* cochlea with less than two turns, vestibule and SCC are hypoplastic.
- *Type IV* cochlea with smaller external dimensions, normal basal turn, and hypoplastic mid and apical turn. Enlarged angle of cisternal and tympanic portion of the VII (also risk of gusher syndrome) (Fig. 2.22) [36].

2.4.10.2 *Labyrinthitis*
CT confirms the end stage of labyrinthine calcifications of scala tympani or scala vestibule or both (Fig. 2.23a).

MRI: Acute labyrinthitis can be seen on MR images as diffuse contrast enhancement of the membranous labyrinth. Later, MRI may show diffuse loss of liquid signal on T2w images due to fibrosis that may not be visible on CT (Fig. 2.23).

2.4.10.3 *Imaging Workup for Cochlear Implant*
As shown in Figs. 2.21, 2.22, and 2.23, CT and MRI of the temporal bones allow excellent depiction of inner ear malformations and are routinely used in the evaluation of pediatric sensorineural hearing loss [43]. However, 80% of congenital SNHL are of membranous origin and will not reveal pathologic findings on imaging [44].
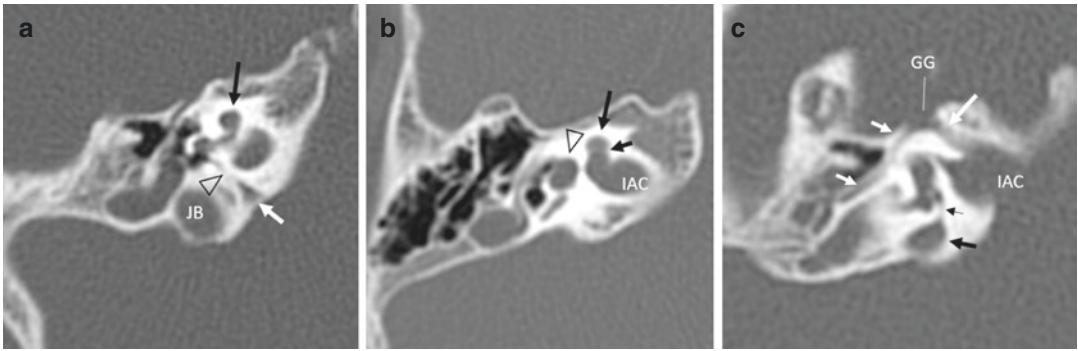
Fig. 2.22 Reconstructed CT images of cochlear hypoplasia type II: (**a**) hypoplastic mid and apical cochlear turns (black arrow). Normal aspect of the cochlear duct, with triangular opening to the posterior fossa (white arrow) anterior to the jugular bulb (JB), very thin aqueduct (arrowhead) until insertion to the basal turn of the cochlear. (**b**) Absent modiolus (short arrow), direct communication between IAC and the hypoplastic cochlea (long arrow), normal sized vestibule (empty triangle). (**c**) Large IAC, enlarged angle at the geniculate ganglion (GG) between the enlarged labyrinthine portion (long white arrow) and tympanic portion (small white arrows) of the VII. Typical LVA (thick black arrow), the proximal isthmic portion is thin (always)
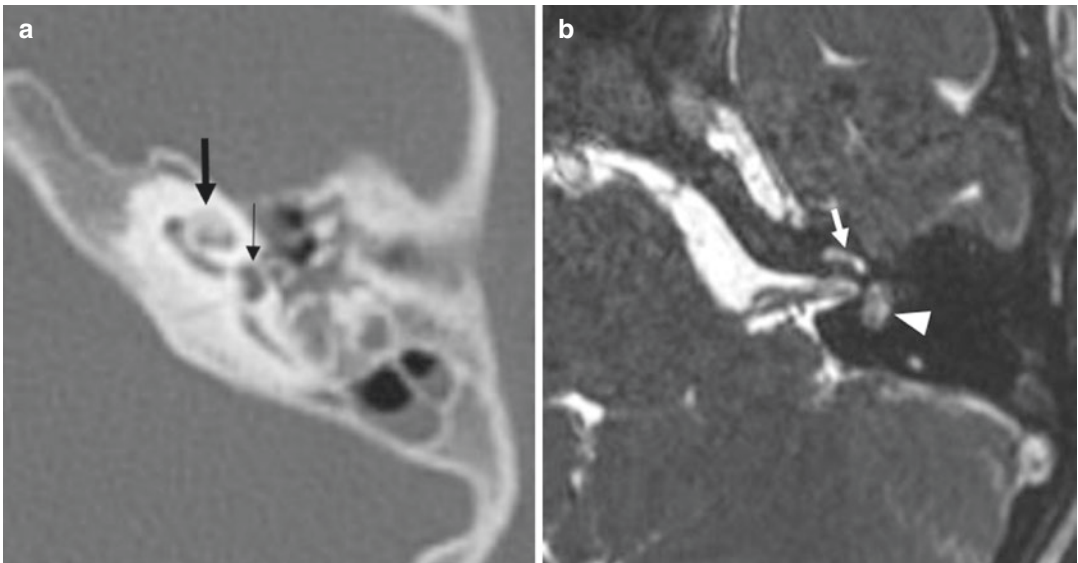

Fig. 2.23 (**a**) Axial CT: calcification of the mid and apical turns of the cochlea (thick arrow). Still normal hypodensity of the vestibule (thin arrow). (**b**) Axial CISS MRI: obscuration of fluid signal intensity in cochlear midturn (arrow), and almost complete absence of liquid signal in the vestibule (arrowhead)

CT may be the exam of first intention that will show an osseous malformation in about 20%.

MRI becomes essential in the workup before cochlear implant, because of its high credibility about

- Patency or obliteration of the cochlear turns.

- Presence of a normally sized cochlear nerve or its absence (Fig. 2.27).
- Absence of lesions of the auditory pathways or the auditory cortex and absence of unexpected associated pathologies which could eventually compromise the long-term safety or function of the cochlear implant.

2.4.11 Cochlear Aqueduct

The cochlear aqueduct has a very thin petrous part arising from the basal turn of the cochlea, to enlarge and widen with a triangular shape at its opening in the subarachnoid space anterior to the jugular foramen (close to the pars nervosa). Only very rare cases of pathologic widening of the whole aqueduct have been reported [45] (Fig. 2.22a).

2.4.12 Vestibule

- Morphology and size of the vestibule can be involved in vestibulocochlear malformations as for example in the incomplete partition type I (Fig. 2.21a).
- Calcifications (rarely in otosclerosis) can appear during ossifying labyrinthitis.

MRI is very sensitive to assess the loss of fluid signal intensity inside the vestibule, corresponding to inflammatory tissue, or fibrosis before calcification (Fig. 2.23b).

The role of 3 Tesla MRI in Menière's disease with delayed acquisition after Gadolinium has already been described in Sect. 2.2.3.2.

2.4.13 Vestibular Aqueduct

Originating from the medial wall of the vestibule, it surrounds the endolymphatic duct. Its proximal part is thin, widening distally, ending in the endolymphatic sac in the posterior fossa. It should not be wider than the superior limb of the PSCC. The Cincinnati criteria [46] consider the vestibular aqueduct as dilated when the mid section of the vestibular aqueduct diameter is greater than 1.0 mm or posterior outside diameter greater than 2.0 mm. LVA (large vestibular aqueduct) is associated to several cochlear or vestibular malformations (Fig. 2.21b), but can also be an isolated finding, and it was found in SNHL of children in 32–39% [46].

2.4.14 Semicircular Canals

- *Anomalies in size or shape* of one or more of the three canals. Complete absence of the posterior labyrinth (Fig. 2.24a) is a rare malformation that is often associated with Charge syndrome [47]. In these cases, arrest of the development must have happened in the 6th gestational week [40]. During the development until the 22nd week, the SSCC forms first, followed by the PSCC and latest the LSCC. However, anomalies of the PSCC (Fig. 2.24b) can be found with a normal LSCC. Anomalies of semicircular canals are the most frequent anomalies found in children with profound hearing loss [48].
- Anomalies of dimension of the canal island are not rare, most often the bony island inside the LSCC is too small (Fig. 2.24c), if inferior to 2.6 mm [49].
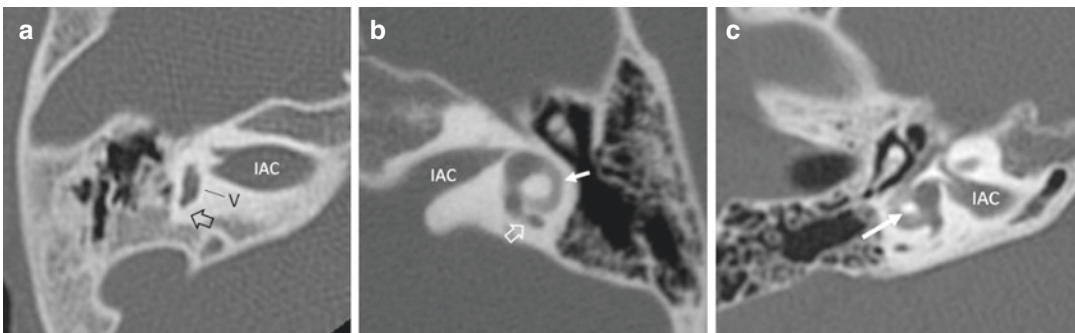

Fig. 2.24 Axial CT-cuts with anomalies of the posterior labyrinth: (**a**) complete absence of the posterior labyrinth (empty arrow) (**b**) very short PSCC (empty arrow), normal LSCC (plain arrow) (**c**) very small bony island of 2 mm inside the LSCC (white arrow). *V* vestibule, *IAC* internal auditory canal
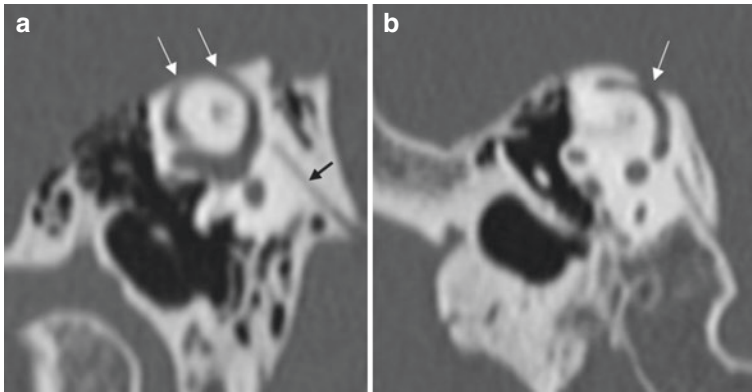
Fig. 2.25 CT Poeschl plan: (**a**) axial CT: dehiscence of the bony cover of the SSCC between the white arrows. Notice also the linear appearance of the vestibular aque-duct in this plan (black arrow). (**b**) Dehiscence of the SSCC with the superior petrosal sinus (arrow)
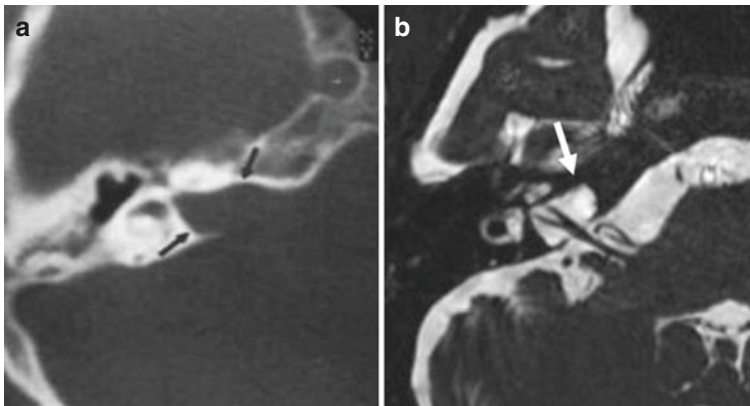

Fig. 2.26 (**a**) Axial CT: enlarged IAC (between arrows), (**b**) axial MR T2w image showing dural ectasia inside the IAC (white arrow)

- Calcification of parts of the lumen, especially after labyrinthitis [50].
- Dehiscence of the bony coverage especially of the SSCC, evaluation on reconstructed images along the Poeschl plan (demonstrated in Fig. 2.4) [51] (Fig. 2.25).

2.4.15 Inner Auditory Canal (IAC)

Normal variants in configuration are funnel shaped, cylindrical, or bud-shaped (Fig. 2.26) [52]. The IAC is considered as stenotic if the diameter is inferior to 2 mm (Fig. 2.27a).

MRI is essential to confirm the presence of the cochlear nerve in case of stenotic IAC (Fig. 2.27b, c) especially before cochlear implant planning (see Sect. 2.4.10).

2.5 Temporal Bone Surfaces: Topographic Pathologies

2.5.1 Lateral Surface

2.5.1.1 *Anomalies of the Auricle*
Usually an indicator of congenital aural dysplasia and not routinely included in the cross-sectional
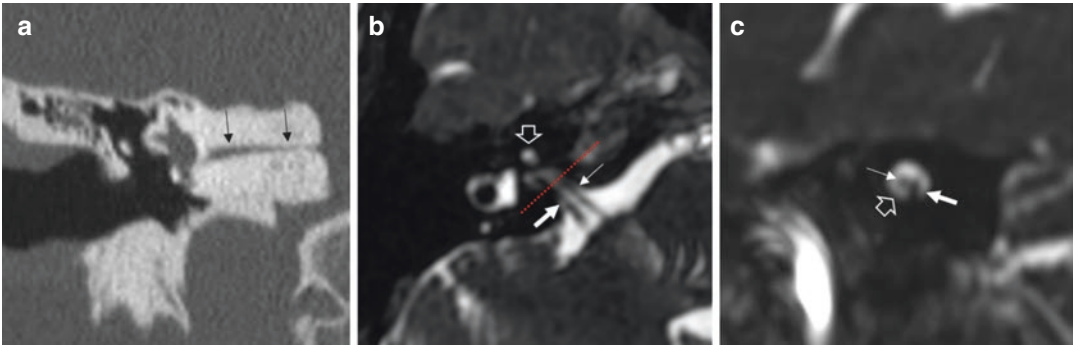
Fig. 2.27 (**a**) Coronal CT: severely stenotic IAC (arrows). (**b**) Axial HR T2w MRI: posteriorly the vestibular nerve (thick arrow) and anteriorly the facial nerve (thin arrow) inside the canal. Rudimentary cochlea type I hypo-plasia (empty arrow). Red reference line for sagittal oblique reconstruction in (**c**): only the vestibular nerves (thick arrow) and the VII (thin arrow) are present, absence of the cochlear nerve (empty arrow)
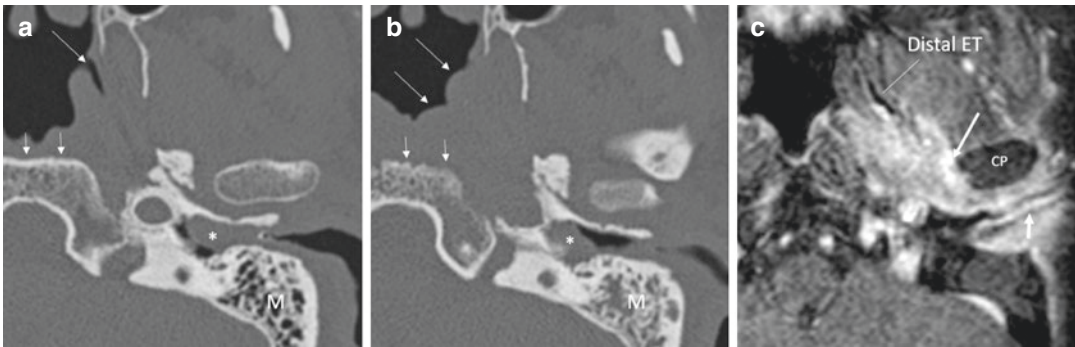

Fig. 2.28 Patient with painful external necrotizing otitis. (**a**) Initial axial CT: condensations confined to EAC (asterisk), intact clivus (white arrows), well aerated mastoid (M). (**b**) Six months later, persistent pain: condensations progressed into the ME cleft (asterisk), lysis of the anterior cortex of the clivus (short arrows). Swelling of nasopharyngeal walls (long arrows). (**c**) T1 w SPIR post Gd MR with important contrast uptake along the EAC (short arrow), inside the temporomandibular joint (long arrow) around the condyloid process (CP) and surrounding the proximal Eustachian tube (ET) that is a virtual lumen in the posterior continuity with the distal ET

imaging unless for special requests in tumor or plastic surgery.

Role of MR permits detailed analyses of the auricle and evaluation of eventual intraosseous extension of skin tumors after i.v. injection of gadolinium.

2.5.1.2 *External Necrotizing Otitis*

CT is often the first approach and may show in the beginning of the process only soft-tissue thickening in the EAC in spite of heavy otalgia (Fig. 2.28a).

Pathways of Infection Spread
- Anteriorly through the fissures of Santorini to the fatty tissue of the temporomandibular joint

(Fig. 2.28b, c) that becomes thickened, to the masticator space, to the parotid.
- Anteromedially to the para-nasopharyngeal fatty tissue with obliteration of the normal fat planes.
- Further medially to the preclival fatty tissue and spreading over the midline to the contra-lateral side with lysis of the clivus cortex as sign of osteomyelitis of the skull base (Fig. 2.28b). This is a sign of advanced disease, often complicated by superior involvement of the skull base and inferior cranial nerves, especially IX, X, and X [53].
- Administration of i.v. iodine contrast is not helpful, because the uptake of inflammatory tissues does not show on CT.

MR, in contrary, is highly superior to evaluate the exact anatomical location and extent of soft-tissue infiltration/infection especially with T1 w post Gadolinium (fat sat) [54] (Fig. 2.28c).

2.5.1.3 *Subperiosteal Abscess*
In the context of acute otomastoïditis, one extratemporal complication along the lateral mastoid surface (Fig. 2.29) is the subperiosteal abscess that concerns most often children.

CT is the first imaging method of choice, usually indicated when intracerebral complications are suspected, showing the lack of trabeculations in the mastoid/antrum, and often small erosions of the bony walls of the mastoid. It should be done with i.v. contrast administration to show subperiosteal collection lateral to the mastoid.

2.5.2 Posterior Surface

2.5.2.1 *Extratemporal Intracranial Complications of CSOM*
CT: Extratemporal spread of infection from the mastoid posteriorly may cause epidural collections in close proximity to the sigmoid sinus (Fig. 2.29a), or even intracerebral abscess formations. Contrast injection is needed!

MR: Sigmoid sinus thrombosis can occur (Fig. 2.29b), best confirmed on MR venography (Fig. 2.29c), that is an imaging technique based on the flow void volume on T2, *without need of intravenous contrast injection*.

2.5.2.2 Endolymphatic Sac
The normal endolymphatic sac is often very small. MR is the only method to visualize the endolymphatic sac.
• *Endolymphatic sac tumors* are very rare.
CT: soft-tissue masses with prominent intratumoral calcifications and permeative bone erosions along the posterior surface of the petrous bone [55].

MR: heterogeneous signal intensity on both T1- and T2-weighted images [56].

2.5.2.3 IAC Meatus and the Cerebellopontine Angle
MR is the method of choice: large differential diagnosis in case of tumors of the IAC/CPA angle (most frequently *vestibular schwannoma* in 60–90%, and *meningioma*, rarely *epidermoid* or *hemangioma* [57, 58].

MR: Inside the IAC, vestibular schwannoma appears iso (35%) or slightly hypointense (65%) to brain tissue on T1w images, strongly enhancing after Gd administration (Fig. 2.30 [59].

2.5.3 Superior Surface

2.5.3.1 Tegmen Tympani
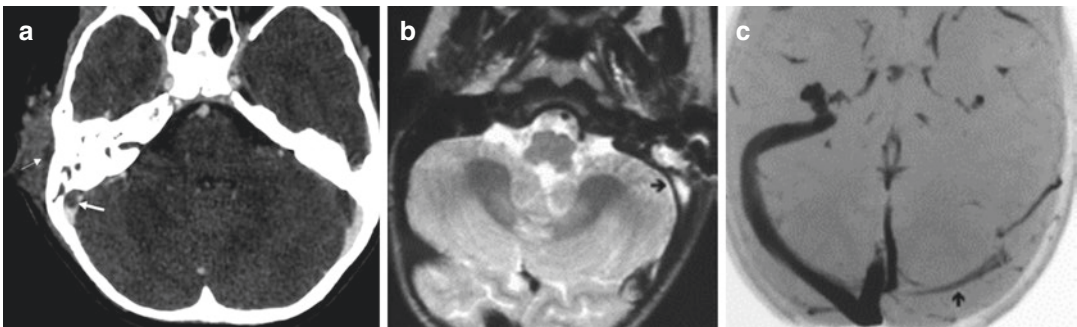It is the lateral aspect of the superior surface, part of the floor of the middle cranial fossa.

Fig. 2.29 (**a**) Axial CT in a young child after i.v. contrast showing a lateral subperiosteal collection (thin arrow) and also posterior extradural collection, that is insinuating in the sigmoid sinus (SS, thick arrow). (**b** and **c**) Another adult patient with left otomastoïditis complicated by SS - thrombosis: (**b**) hyperintense aspect of thrombotic clot in the SS (arrow), (**c**) typical image of left SS - thrombosis (arrow) on MR venography
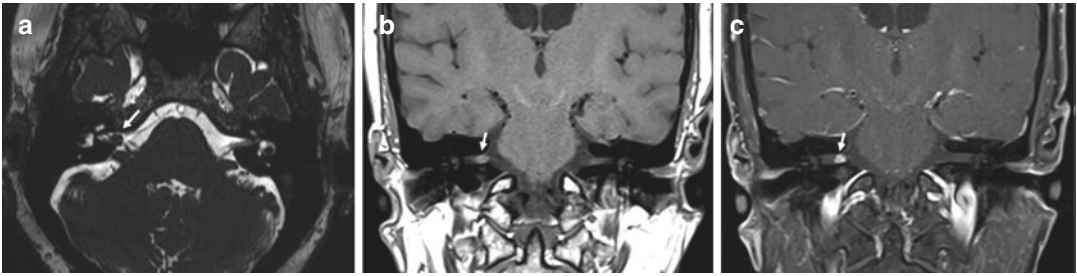
Fig. 2.30 Vestibular intracanalicular schwannoma: (**a**) Axial CISS and (**b**) coronal T1 WI MRI before and (**c**) after i.v. contrast administration: (**a**) small right intracanalicular lesion as lack of fluid signal in the IAC (arrow), (**b**) spontaneously isodense on T1w MR to brain tissue (arrow), (**c**) homogenously enhancing postcontrast (arrow)
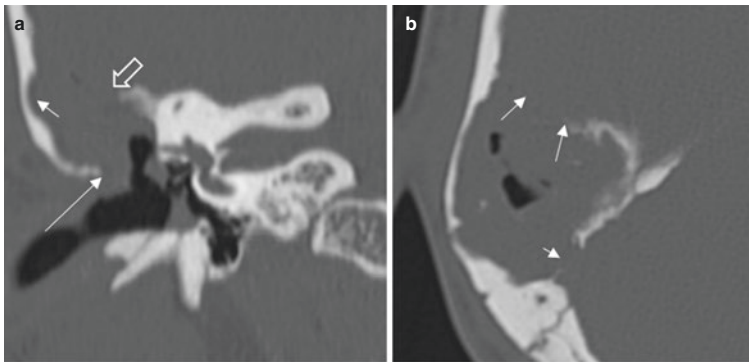

Fig. 2.31 (**a**) Coronal CT: large amputation of the scutum (long arrow) and huge soft-tissue mass (cholesteatoma) occupying the whole attic, and extending into the middle cranial fossa through a large tegmen defect, causing scalloping of the lateral skull (short small arrow). (**b**) Axial CT showing the huge mass at the level of the lytic tegmen, almost complete lysis of the anterior limit (long arrows) and posterior limit (short arrow)

CT: Extension of an ME cholesteatoma through a lytic or dehiscent tegmen into the middle cranial fossa can be already obvious by CT (Fig. 2.31).

MR: In case of discontinuity of the tegmen and nonspecific soft-tissue densities in the middle ear cleft, MRI can show *meningoencephalocele* herniating into the ME (Fig. 2.32) that may be spontaneous, or coexist with a cholesteatomatous process inside the ME cleft.

Also CSF leak through a tegmen defect causing otoliquorrhea can be suspected on CT but needs the diagnostic contribution of MR for the eventual underlying conditions. Proof of this communication can be done by intrathecal injection of contrast and demonstration of the contrast inside the middle ear cleft [60].

2.5.3.2 Geniculate Ganglion and Greater Superficial Petrosal Nerve

- Most frequent pathologies of these nervous structures are *schwannomas or hemangiomas*, both are well demonstrated by *MR with Gd*.
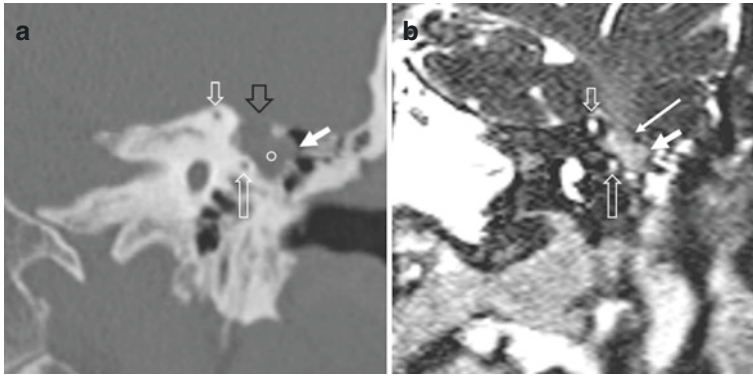
Fig. 2.32 (**a**) Coronal CT: tegmen discontinuity (empty black arrow), obliteration of the attic with convex borders (thick arrow). Density measurement of this condensation (circle) is 1 UH, corresponding to liquid! (**b**) Coronal HR T2w MR showing continuity of cerebral tissue (long arrow) into the superior attic and moderately hyperintense fluid signal in the underlying sac (thick arrow), representing meningoencephalocele. For (**a** and **b**): *SSCC* short empty arrow, *LSCC* long empty arrow
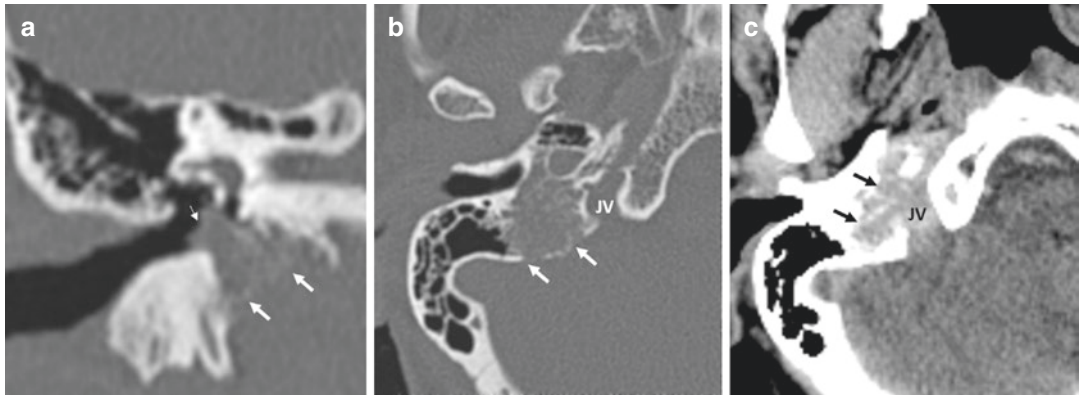

Fig. 2.33 Coronal CT: (**a**) hypotympanic soft-tissue mass (small arrow), diffuse infiltration of the posteroinferior mastoid (thick arrows) (**b**) axial CT diffuse infiltration of the inferior mastoid (arrows). *JV* jugular vein. (**c**) Axial post-contrast CT, diffuse enhancement of the jugulotympanic glomus tumor (arrows)

2.5.4   Inferior Surface

- Posterior boundary of the mandibular fossa
    - Thickening of soft tissue, erosions as sign of eventual spread of infectious diseases
- Jugular foramen, foramen of the carotid artery, numerous cranial nerves passing through the pars nervosa (Nerfs IX, X, XI), and their pathologies

2.5.4.1   *Glomus Tumor*

CT: shows almost always a bulging soft-tissue mass in the hypotympanum typically with important contrast uptake, associated to erosive lesions of the mastoid adjacent to the jugular bulb (Fig. 2.33).

MRI: permits to precise the extension from the glomus of the tympanic nerve to the nerfs of the jugular foramen and extension at the base of skull [61].

2.6 Input of Postoperative Imaging/Follow-Up

Tympanostomies and tympanoplasties do not require scanographic evaluation unless complications. Tympanoplasty leads often to an opaque TM that does not permit otoscopic analysis of the underlying structures. CT permits to reveal retrotympanic processes as developing cholesteatoma (Fig. 2.34a).

2.6.1 Ossicular Reconstruction (Incus Interposition, PORP/TORP)

Incus interposition appears with typical ossicular density but modified in form and position, establishing a continuity between TM and stapes. **PORP and TORP** are synthetic prostheses that engage laterally with the TM, medially with the stapes superstructure (PORP, Fig. 2.34b) or directly with the footplate (TORP). Displacement can be demonstrated by CT (Fig. 2.34c).

CBCT: some studies demonstrated a good visibility of the TORP and analysis of its distal positioning on the footplate with the help of three-dimensional CBCT reformatting [62].

2.6.2 Stapes Prosthesis

CT: Some prostheses are very dense on CT, causing streak artifacts, that should not be mistaken for fibrotic bands (Fig. 2.35a). Metallic artifacts yield to a 0.5 mm overestimation of size and intravestibular length of metallic prosthesis with conventional CT scan [63].

Other types of prosthesis appear with much lower density and do not produce artifacts (Fig. 2.35b).

The prosthesis may have lost the contact with the long incus process (empty loop sign, Fig. 2.35b). The tip of the prosthesis may be deviated on the footplate or show a deep insertion into the vestibule (Fig. 2.35b). Recurrence of the otosclerotic process around the footplate or fibrous bands that cause relapse of fixity can be seen by CT [64, 65].

Also CT can demonstrate pneumolabyrinth as a stapedotomy complication [66].

MR: can give precision about intravestibular pathologies:
- Granuloma development with inflammatory labyrinthitis, typically with intermediate T1, hypointense T2w images, and contrast enhancement post Gd.
- Intra labyrinthine hemorrhage (hyperintense in T1 and T2).
- Suppurative labyrinthitis with intense Gd enhancement [67].
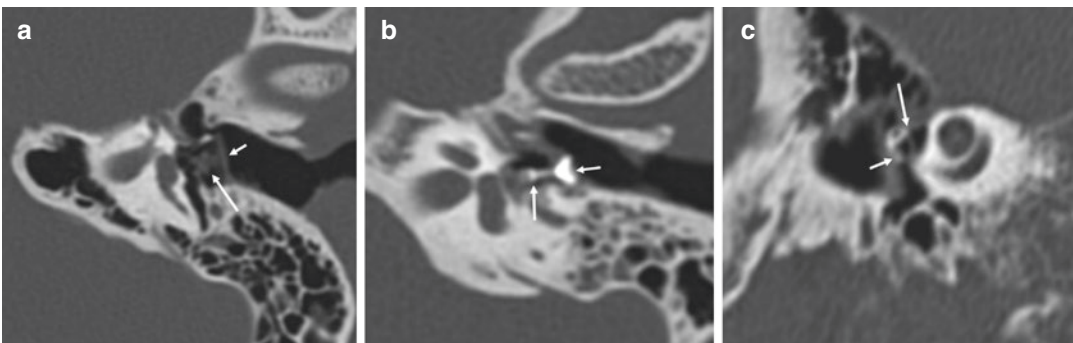

Fig. 2.34 CT of (**a**) Tympanoplasty as a thick linear structure (short arrow), hiding mesotympanic cholesteatoma formation (long arrow). (**b**) PORP with satisfactory contact with the TM (short arrow), medially with the stapes head (arrow). (**c**) Displaced PORP, only partially in contact with the TM (short arrow), its distal tip is disconnected (long arrow)
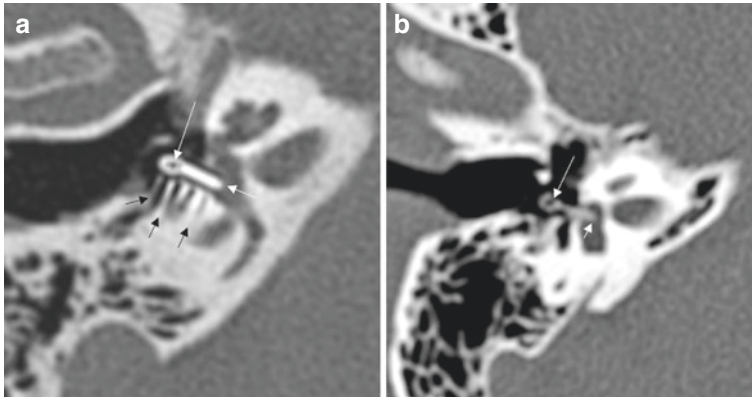
Fig. 2.35 CT reconstructed in the axial stapes plan of two different types of stapes prosthesis: (**a**) prosthesis of titanium, the ring (long arrow) shows a black center due to high density artifact (it is not empty). Multiple streak artifacts (small black arrows). Tip of prosthesis (white short arrow) enters about 1/3 of transversal diameter into the vestibule. (**b**) Another type of prosthesis is less dense, showing a real empty loop (long arrow). The distal tip is far advanced into the vestibule, about 2/3 of the transversal diameter
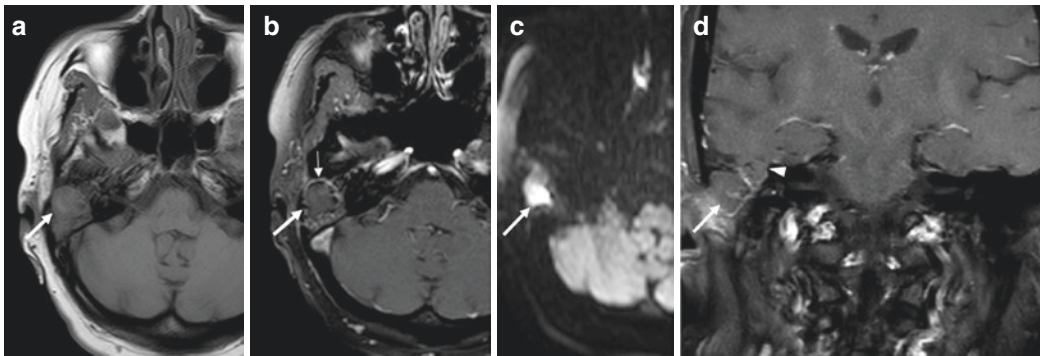

Fig. 2.36 (**a**) ax T1w MR: large atticoantral isointense lesion (arrow), (**b**) ax T1w MR with Gd, no contrast uptake (thick arrow) but thin surrounding rim enhancement (small arrow). (**c**) DW B1000 image: strong restriction (arrow) confirming cholesteatoma. (**d**) On coronal T1wMR: associated meningoencephalocele (arrowhead), medial to the cholesteatoma (arrow)

2.6.3 Recurrent/Residual Cholesteatoma

CT has a high negative predictive value in a well-aerated middle ear cleft with no evidence of abnormal soft tissue [68]. Recurrent cholesteatoma is suspected, when soft-tissue formations are associated to new bone erosions on comparative studies, although the attenuation characteristics are nonspecific.

MR: As diffusion-weighted images have a high predictive value for residual/recurrent cho-lesteatoma (see Sects. 2.2.3.2 and 2.4.3), non-EPI DWI MR may help to classify patients into groups with indication for second look surgery versus follow up [69, 70].

However, the MR exploration must always include conventional sequences to avoid false-positive interpretations from eventual fat grafts or hemorrhage [71], and to search for associated anomalies that are important to consider during surgery, as associated meningoencephalocele (Fig. 2.36).
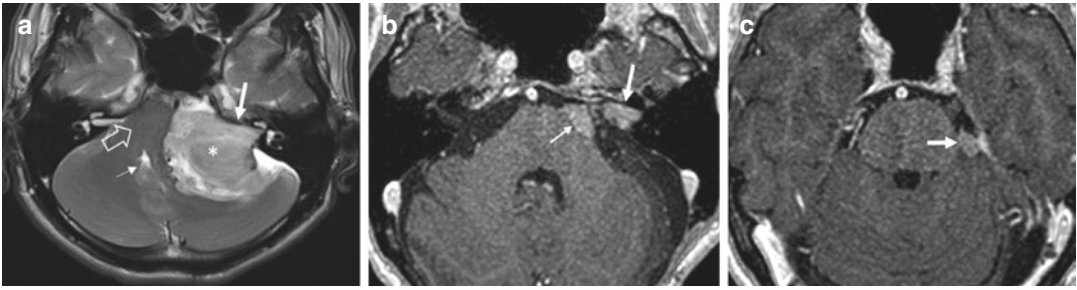
Fig. 2.37 Axial MR T1w after Gd: (**a**) initially huge vestibular schwannoma occupying the whole IAC (white thick arrow) and CPA angle (asterisk) with important mass effect on the pons (empty arrow) and forth ventricle (small arrow). (**b**) Postoperative residual tissues left in the IAC (thick arrow), in close contact with the pons (small arrow) and (**c**) in the upper posterior angle of the cerebellopontine cisterna (arrow) 2 years after subtotal resection with facial nerve preservation

2.6.4 Vestibular Schwannoma

MRI is routinely performed after resection as base line exploration, to assess residual or recurrent tumor, as well as for suspected complications, as there are fat graft necrosis, CSF leakage, infection, cerebral infarction, venous sinus thrombosis, hemorrhage, cerebellar atrophy, and endolymphatic fluid loss [72]

- Almost every first control by MRI shows residual enhancement in the surgical bed.
  - If the enhancement is linear, it is mainly corresponding to scar and/or granulation tissue and can persist for 1 year or longer.
  - If the enhancement is nodular, it is almost always residual tissue [73] (Fig. 2.37). Very exact reproducible measurements are necessary over time to evaluate disease progression for these slow growing processes.

2.7 Conclusion

Temporal bone imaging is considered nowadays the main diagnostic tool to enrich the clinical and therapeutical approaches. It orients surgical indications and helps to anticipate eventual abnormalities or complications that may modify the surgical outcome. Several imaging tools are available for most dedicated imaging, and this chapter emphasizes the utility of CT versus MR imaging depending on the clinical evaluation and course of the disease. CT and MRI are complementary methods, both can be often necessary to elucidate several pathologies. Constant feedback between otologist and radiologist is a key to improve our experience regard to ear disease management.

Take-Home Messages
- CT is the first imaging modality for middle ear pathologies with conductive hearing loss, especially in otosclerosis, tympanosclerosis, chronic suppurative otitis media, cholesteatoma, SSCC dehiscence, or congenital malformations.
- In the postoperative follow-up, CT demonstrates especially prosthesis status (preferably by CBCT when available) and follow-up of otosclerosis progress.
- MRI better differentiates doubtful middle ear condensations that are suspicious for cholesteatoma, recurrence of cholesteatoma, and extension beyond the limits of the temporal bone of any infectious or tumoral process.
- MRI is the key imaging method to analyze the content of IAC and of CPA. It is part of the systematic workup before cochlear implant.
- CT and MRI are often complementary methods. A constant collaboration between otologist and radiologist is essential to improve imaging diagnosis for better ear disease management.

References

1. Gentric JC, Rousset JR, Garetier M, Ben Salem D, Meriot P. High-resolution computed tomography of isolated congenital anomalies of the stapes: a pictural review using oblique multiplanar reformation in the "axial stapes" plane. J Neuroradiol. 2012;39(1):58–64.

2. Lemmerling M, de Foer B. Temporal bone imaging. New York: Springer; 2014.

3. Daly MJ, Siewerdsen JH, Moseley DJ, et al. Intraoperative cone-beam CT for guidance of head and neck surgery: assessment of dose and image quality using a C-arm prototype. Med Phys. 2006;33:3767–80.

4. Loubele M, Bogaerts R, Van Dijck E, et al. Comparison between effective radiation dose of CBCT and MSCT scanners for dentomaxillofacial applications. Eur J Radiol. 2009;71:461Y8.

5. Miracle AC, Mukherji SK. Conebeam CT of the head and neck, Part 1: Physical principles. AJNR Am J Neuroradiol. 2009;30(6):1088–95.

6. Mori S, Endo M, Nishizawa K, et al. Enlarged longitudinal dose profiles in cone-beam CT and the need for modified dosimetry. Med Phys. 2005;32:1061–9.

7. Kyriakou Y, Deak P, Langner O, et al. Concepts for dose determination in flat-detector CT. Phys Med Biol. 2008;53:3551–66. Epub 2008 Jun 13.

8. Gupta R, Bartling SH, Basu SK, et al. Experimental flat-panel high-spatial resolution volume CT of the temporal bone. AJNR Am J Neuroradiol. 2004;25:1417–24.

9. Dahmani-Caussea M, Marxa M, Deguinea O, Frayssea B, Lepageb B, Escudé B. Morphologic examination of the temporal bone by cone beam computed tomography: comparison with multislice helical computed tomography. Eur Ann Otorhinolaryngol Head Neck Dis. 2011;128(5):230–5.

10. Miracle AC, Mukherji SK. Conebeam CT of the head and neck, Part 2: Clinical applications. AJNR Am J Neuroradiol. 2009;30:1285–92.

11. Aschendorff A, Kubalek R, Hochmuth A, et al. Imaging procedures in cochlear implant patients: evaluation of different radiological techniques. Acta Otolaryngol Suppl. 2004;552:46–9.

12. Ruivo J, Mermuys K, Bacher K, Kuhweide R, Offeciers E, Casselman JW. Cone beam computed tomography, a low-dose imaging technique in the postoperative assessment of cochlear implantation. Otol Neurotol. 2009;30(3):299–303. https://doi.org/10.1097/mao.0b013e31819679f9.

13. Révész P, Liktor B, Liktor B, Sziklai I, Gerlinger I, Karosi T. Comparative analysis of preoperative diagnostic values of HRCT and CBCT in patients with histologically diagnosed otosclerotic stapes footplates. Eur Arch Oto-Rhino-Laryngol. 2016;273(1):63–72. 10p.

14. Redfors YD, Gröndahl HG, Hellgren J, Lindfors N, Nilsson I, Möller C. Otosclerosis: anatomy and pathology in the temporal bone assessed by multi-slice and cone-beam CT. Otol Neurotol. 2012;33:922–7.

15. Mangrum W, Christianson K, Duncan S, et al. Duke review of MRI principles. Philadelphia, PA: Mosby; 2012.

16. Dremmen MH, Hofman PA, Hof JR, Stokroos RJ, Postma AA. The diagnostic accuracy of non-echo-planar diffusion weighted imaging in the detection of residual and/or recurrent cholesteatoma of the temporal bone. AJNR Am J Neuroradiol. 2012;33:439–44.

17. Dudau C, Draper A, Gkagkanasiou M, Charles-Edwards G, Pai I, Connor S. Cholesteatoma: multishot echo-planar vs non echo-planar diffusion-weighted MRI for the prediction of middle ear and mastoid cholesteatoma. BJR Open. 2019;1:20180015.

18. Naganawa S, Satake H, Iwano S, Fukatsu H, Sone M, Nakashima T. Imaging endolymphatic hydrops at 3 tesla using 3DFLAIR with intratympanic Gd-DTPA administration. Magn Reson Med Sci. 2008;7(2):85–91.

19. Venkatasamy A, Veillon F, Fleury A, Eliezer M, Abu Eid M, Romain B, Vuong H, Rohmer D, Charpiot A, Sick H, Riehm S. Imaging of the saccule for the diagnosis of endolymphatic hydrops in Meniere disease, using a three-dimensional T2-weighted steady state free precession sequence: accurate, fast, and without contrast material intravenous injection. Eur Radiol Exp. 2017;1:14.

20. Bernaerts B, Vanspauwen R, Blaivie C, van Dinther J, Zarowski A, Wuyts F, Vanden Bossche S, Offeciers E, Casselman JW, De Foer B. The value of four stage vestibular hydrops grading and asymmetric perilymphatic enhancement in the diagnosis of Menière's disease on MRI. Neuroradiology. 2019;61:421–9.

21. Fritsch M. MRI scanners and stapes prosthesis. Otol Neurotol. 2007;28:733–8.

22. Syms MJ. Safety of magnetic resonance imaging of stapes prostheses. Laryngoscope. 2005;115:381–90.

23. Mansour S, Magnan J, Nicolas K, Haidar H. Middle ear diseases. New York: Springer; 2018. p. 471–73.

24. Patil AR, Bhalla A, Gupta P, et al. HRCT evaluation of microtia: a retrospective study. Indian J Radiol Imaging. 2012;22(3):188–94.

25. Gassner EM, Mallouhi A, Jaschke WR. Preoperative evaluation of external auditory canal atresia on high-resolution CT. AJR Am J Roentgenol. 2004;182(5):1305–12.

26. Mansour S, Magnan J, Haidar H, Nicolas K. Tympanic membrane retraction pocket, overview and advances in diagnosis and management. New York: Springer; 2015.

27. Mansour S, Magnan J, Haidar H, Nicolas K, Louryan S. Comprehensive and clinical anatomy of the middle ear. 2nd ed. New York: Springer; 2019. p 44.

28. Li P, Linos E, Gurgel R, Fischbein N, Blevins N. Evaluating the utility of non–echo-planar diffusion-weighted imaging in the preoperative evaluation of cholesteatoma: a meta-analysis. Laryngoscope. 2013;123:1247–50.

29. Lingam R, Bassett P. A meta-analysis on the diagnostic performance of non-echoplanar diffusion-weighted

imaging in detecting middle ear cholesteatoma: 10 years on. Otol Neurotol. 2017;38:521–8.

30. Jindal M, Riskalla A, Jiang D, Connor S, O'Connor AF. A systematic review of diffusion-weighted magnetic resonance imaging in the assessment of postoperative cholesteatoma. Otol Neurotol. 2011;32:1243–49.

31. Mansour S, Magnan J, Nicolas K, Haidar H. Middle ear diseases. New York: Springer; 2018 chapter tympanosclerosis pages 169-181 and/or chapter otosclerosis pages 1-33.

32. Lagleyre S, Sorrentino T, Calmels MN, Shin YJ, Escudé B, Deguine O, Fraysse B. Reliability of high-resolution CT scan in diagnosis of otosclerosis. Otol Neurotol. 2009;30(8):1152–9.

33. Veillon F, Stierle JL, Dussaix J, et al. Otosclerosis imaging: matching clinical and imaging data. J Radiol. 2006;87:1756–64.

34. Marshall AH, Fanning N, Symons S, Shipp D, Chen JM, Nedzelski JM. Cochlear implantation in cochlear otosclerosis. Laryngoscope. 2005;115:1728–33.

35. Mansour S, Nicolas K, Ahmad HH. Round window otosclerosis: radiologic classification and clinical correlations. Otol Neurotol. 2011;32(3):384–92.

36. Sennaroglu L, Bajin MD, Pamuk E, Tahir E. Cochlear hypoplasia type four with anteriorly displaced facial nerve canal. Otol Neurotol. 2016;37:407–9.

37. Gupta S, Mends F, Hagiwara M, Fatterpekar G, Roehm PC. Imaging the facial nerve: a contemporary review. Radiol Res Pract. 2013;2013:248039. 14 pages.

38. Mansour S, Magnan J, Nicolas K, Haidar H. Middle ear diseases. New York: Springer; 2018. p. 296–300.

39. Razek AA, Huang BY, et al. Lesions of the petrous apex: classification and findings at CT and MR imaging. Radio Graphics. 2012;32:151–73.

40. Jackler RK, Luxford WM, House WF. Congenital malformations of the inner ear: a classification based on embryogenesis. Laryngoscope. 1987;97:2–14.

41. Sennaroglu L, Saatci I. A new classification for cochleovestibular malformations. Laryngoscope. 2002;112:230–41.

42. Sennaroglu L. Cochlear implantation in inner ear malformations – a review article. Cochlear Implants Int. 2009;11(1):4–41.

43. Joshi V, Navlekar SK, Kishore G, Reddy K, Kumar E. CT and MR imaging of the inner ear and brain in children with congenital sensorineural hearing loss. Radiographics. 2012;32:683–98.

44. Sennaroğlu L, Bajin M. Classification and current management of inner ear malformations. Balkan Med J. 2017;34:397–411.

45. Mukherji SK, Baggett HC, Alley J, Carrasco VH. Enlarged cochlear aqueduct. AJNR Am J Neuroradiol. 1998;19:330–2.

46. Vijayasekaran S, Halsted MJ, Boston M, Meinzen-Derr J, Bardo DME, Greinwald J, Benton C. When is the vestibular aqueduct enlarged? A statistical analysis of the normative distribution of vestibular aqueduct size. Am J Neuroradiol. 2007;28(6):1133–8.

47. Morimoto AK, Wiggins RH III, Hudgins PA, Hedlund GL, Hamilton B, Mukherji SK, Telian SA, Harnsberger HR. Absent semicircular canals in CHARGE syndrome: radiologic spectrum of findings. AJNR Am J Neuroradiol. 2006;27(8):1663–71.

48. Wu WJ, He XB, Tan LH, Hu P, Peng AO, Xiao ZA, Yang S, Wang T, Qing J, Chen X, Li JK, Peng T, Dong YP, Liu XZ, Xie DH. Imaging assessment of profound sensorineural deafness with inner ear anatomical abnormalities. J Otol. 2015;10:29–38.

49. Purcell D, Fischbein N, Patel A, Johnson J, Lalwani A. Two temporal bone computed tomography measurements increase recognition of malformations and predict sensorineural hearing loss. Laryngoscope. 2006;116:1439–46.

50. Lemmerling M, Vanzieleghem B, Dhooge I, Van Cauwenberge P, Kunnen M. CT and MRI of the semicircular canals in the normal and diseased temporal bone. Eur Radiol. 2001;11:1210–9.

51. Minor LB, Solomon D, Zinreich JS, Zee DS. Sound- and/or pressure-induced vertigo due to bone dehiscence of the superior semicircular canal. Arch Otolaryngol Head Neck Surg. 1998;124:249–58.

52. Marques S, Ajzen S, D'Ippolito G, Alonso L, Isotani S, Lederman H. Morphometric analysis of the internal auditory canal by computed tomography imaging. Iran J Radiol. 2012;9(2):71–8.

53. Mani N, Sudhoff H, Rajagopal S, Moffat D, Axon P. Cranial nerve involvement in malignant external otitis: implications for clinical outcome. Laryngoscope. 2007;117:907–10.

54. van Kroonenburgh A, van der Meer WL, Bothof RJP, van Tilburg M, van Tongeren J, Postma AA. Advanced imaging techniques in skull base osteomyelitis due to malignant otitis externa. Curr Radiol Rep. 2018;6:3.

55. Kumar M, Ramakrishnaiah R, Muhhamad Y, Van Hemert R, Angtuaco E. Endolymphatic sac tumor. Radiol Case Rep. 2011;6(3).

56. Sun YH, Wen W, Wu JH, Song JM, Guan H, Wang KX, Xu MQ. Endolymphatic sac tumor: case report and review of the literature. Diagn Pathol. 2012;7:36.

57. Casselman J, Lu CH, De Foer B, Delanote J. Schwannomas of the cochleo-vestibular nerve (Schwannomes du nerf vestibulo-cochléaire). In: Veillon F, editor. Imagerie de l'oreille et de l'os temporal. Tome 4, chapitre 26. Paris: Lavoisier; 2013. p. 921–57.

58. Bonfort G, Veillon F, Debry C, Kehrli P, Chibbaro S. VIIIth nerve cavernous hemangioma mimicking a stage 1 acoustic schwannoma. Neurochirurgie. 2015;61:352–5.

59. Mulkens TH, Parizel PM, Martin JJ, et al. Acoustic schwannoma: MR findings in 84 tumors. AJR Am J Roentgenol. 1993;160(2):395–8.

60. Schubiger O, Valvanis A, Stuckmann G, Antonucci F. Temporal bone fractures and their complications: examination with high resolution CT. Neuroradiology. 1986;28:93–9.

61. Mravic M, LaChaud G, Nguyen A, Scott M, Dry S, James A. Clinical and histopathological diagnosis of glomus tumor: an institutional experience of 138 cases. Int J Surg Pathol. 2015;23(3):181–8.

62. Komori M, Yanagihara N, Hyodo J, Miuchi S. Position of TORP on the stapes footplate assessed with cone beam computed tomography. Otol Neurotol. 2012;33:1353–6.

63. Warren FM, Riggs S, Wiggins RH III. Computed tomographic imaging of stapes implants. Otol Neurotol. 2008;29:586–92.

64. Ali HI, Khater NH. Otosclerosis and complications of stapedectomy: CT and MRI correlation Alexandria. J Med. 2018;54:197–201.

65. Kösling K, Plontke SK, Bartel S. Imaging of otosclerosis. Fortschr Röntgenstr. 2020; https://doi.org/10.1055/a-1131-7980.

66. Ziade G, Barake R, El Natout T, El Natout M-A. Late pneumolabyrinth after stapedectomy. Eur Ann Otorhinolaryngol Head Neck Dis. 2016;133(5):361–3.

67. Rangheard AS, Marsot-Dupuch K, Mark A, Meyer B, Tubiana JM. Postoperative complications in oto-spongiosis: usefulness of MR imaging. AJNR Am J Neuroradiol. 2001;22:1171–8.

68. Barath K, Huber AM, Stämpfli P, Varga Z, Kollias S. Neuroradiology of cholesteatomas. AJNR Am J Neuroradiol. 2010;32:221–9.

69. Keeler JA, Kaylie DM. Cholesteatoma: is a second stage necessary? Laryngoscope. 2016;126:1499–500.

70. Steens S, Venderink W, Kunst D, Meijer A, Mylanus E. Repeated postoperative follow-up diffusion-weighted magnetic resonance imaging to detect residual or recurrent cholesteatoma. Otol Neurotol. 2016;37:356–61.

71. Juliano AF, Ginat DT, Moonis G. Imaging review of the temporal bone: Part II. Traumatic, postoperative, and noninflammatory nonneoplastic conditions. Radiology. 2015;276:655–72.

72. Ginat DT, Martuza RL. Postoperative imaging of vestibular schwannomas. Neurosurg Focus. 2012;33:E18.

73. Carlson ML, Van Abel KM, Driscoll CL, et al. Magnetic resonance imaging surveillance following vestibular schwannoma resection. Laryngoscope. 2012;122:378–88.